

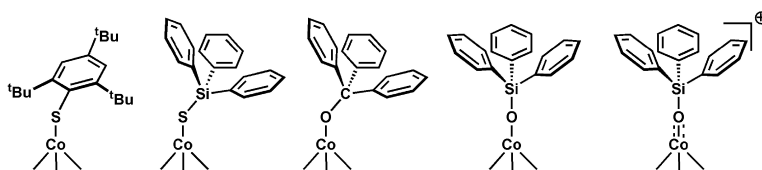
Article

Spin-State Tuning at Pseudotetrahedral d Ions: Examining the Structural and Magnetic Phenomena of Four-Coordinate [BP]Co–X Systems

David M. Jenkins, and Jonas C. Peters

J. Am. Chem. Soc., **2005**, 127 (19), 7148-7165 • DOI: 10.1021/ja045310m • Publication Date (Web): 20 April 2005

Downloaded from <http://pubs.acs.org> on March 25, 2009



More About This Article

Additional resources and features associated with this article are available within the HTML version:

- Supporting Information
- Links to the 13 articles that cite this article, as of the time of this article download
- Access to high resolution figures
- Links to articles and content related to this article
- Copyright permission to reproduce figures and/or text from this article

[View the Full Text HTML](#)



ACS Publications
 High quality. High impact.

Spin-State Tuning at Pseudotetrahedral d^7 Ions: Examining the Structural and Magnetic Phenomena of Four-Coordinate $[\text{BP}_3]\text{Co}^{\text{II}}-\text{X}$ Systems

David M. Jenkins and Jonas C. Peters*

Contribution from the Division of Chemistry and Chemical Engineering, Arnold and Mabel Beckman Laboratories of Chemical Synthesis, California Institute of Technology, Pasadena, California 91125

Received August 3, 2004; E-mail: jpeters@caltech.edu

Abstract: Electronic structure, spin-state, and geometrical relationships for a series of pseudotetrahedral Co(II) aryloxide, siloxide, arylthiolate, and silylthiolate complexes supported by the tris(phosphino)borate $[\text{BP}_3]$ ligands $[\text{PhBP}_3]$ and $[\text{PhBP}^{\text{Pr}_3}]$ ($[\text{PhB}(\text{CH}_2\text{PPh}_2)_3]^-$ and $[\text{PhB}(\text{CH}_2\text{P}^{\text{Pr}})_2)_3]^-$, respectively) are described. Standard ^1H NMR, optical, electrochemical, and solution magnetic data, in addition to low-temperature EPR and variable temperature SQUID magnetization data, are presented for the new cobalt(II) complexes $[\text{PhBP}_3]\text{CoOSiPh}_3$ (**2**), $[\text{PhBP}_3]\text{CoO}(4\text{-}^i\text{Bu-Ph})$ (**3**), $[\text{PhBP}_3]\text{CoO}(\text{C}_6\text{F}_5)$ (**4**), $[\text{PhBP}_3]\text{CoSPh}$ (**5**), $[\text{PhBP}_3]\text{CoS}(2,6\text{-Me}_2\text{-Ph})$ (**6**), $[\text{PhBP}_3]\text{CoS}(2,4,6\text{-}^i\text{Pr}_3\text{-Ph})$ (**7**), $[\text{PhBP}_3]\text{CoS}(2,4,6\text{-}^i\text{Bu}_3\text{-Ph})$ (**8**), $[\text{PhBP}_3]\text{CoSSiPh}_3$ (**9**), $[\text{PhBP}_3]\text{CoOSi}(4\text{-NMe}_2\text{-Ph})_3$ (**10**), $[\text{PhBP}_3]\text{CoOSi}(4\text{-CF}_3\text{-Ph})_3$ (**11**), $[\text{PhBP}_3]\text{CoOCPPh}_3$ (**12**), $[\text{PhBP}^{\text{Pr}_3}]\text{CoOSiPh}_3$ (**14**), and $[\text{PhBP}^{\text{Pr}_3}]\text{CoSSiPh}_3$ (**15**). The low-temperature solid-state crystal structures of **2**, **3**, **5**–**10**, **12**, and **15** are also described. These pseudotetrahedral cobalt(II) complexes are classified as featuring one of two limiting distortions, either umbrella or off-axis. Magnetic and spectroscopic data demonstrate that both $S = 1/2$ and $S = 3/2$ ground-state electronic configurations are accessible for the umbrella distorted structure type, depending on the nature of the X-type ligand, its denticity (η^1 versus η^3), and the tripodal phosphine ligand employed. Off-axis distorted complexes populate an $S = 1/2$ ground-state exclusively. For those four-coordinate complexes that populate $S = 1/2$ ground states, X-ray data show two Co–P bond distances that are invariably shorter than a third Co–P bond. The pseudotetrahedral siloxides **2**, **10**, and **11** are exceptional in that they display gradual spin crossover in the solid state. The diamagnetic cobalt(III) complex $\{[\text{PhBP}_3]\text{CoOSiPh}_3\}\{\text{BAR}_4\}$ ($\{\mathbf{16}\}\{\text{BAR}_4\}$) ($\text{Ar} = \text{Ph}$ or $3,5\text{-}(\text{CF}_3)_2\text{-C}_6\text{H}_3$) has also been prepared and structurally characterized. Accompanying electronic structure calculations (DFT) for complexes **2**, **6**, and $\{\mathbf{16}\}^+$ support the notion of a close electronic structure relationship between these four-coordinate systems and octahedral, sandwich, and half-sandwich coordination complexes.

I. Introduction

Stereochemical and electronic structure phenomena of the first-row transition ions are central issues in coordination chemistry. These properties are strongly coupled and the experimental determination of one property often intimates a great deal about the other. For instance, knowledge of a complex's solid-state crystal structure can point to its electronic ground-state configuration. The four-coordinate first-row transition ions Fe(II), Co(II), and Ni(II) are exemplary. Each is high spin when approximately tetrahedral, occupying $S = 2$, $S = 3/2$, and $S = 1$ ground states, respectively. By contrast, when these same ions feature square planar structures, low-spin (Co(II) and Ni(II))¹ or intermediate-spin (Fe(II))² ground states are manifest. Knowledge of the interplay between stereochemistry and electronic structure thus lies at the heart of our ability to anticipate magnetic phenomena from key structural parameters. Indeed, the assignment of local stereochemical environments

within complex metalloenzyme active sites is often achieved by the interpretation of spectroscopic data.^{3,4} Moreover, chemical reactivity can be dramatically effected by subtle spin-state/stereochemical relationships, as in numerous biocatalytic transformations.⁵ Inorganic complexes that expose new insights regarding the relationship between stereochemistry and electronic structure are therefore of broad concern.

From the perspective of ligand field theory (LFT) one of the best-studied transition ions is Co^{2+} .⁶ The most prominent

(1) (a) Nishida, Y.; Kida, S. *Bull. Chem. Soc. Jpn.* **1978**, *51*, 143–149. (b) Gray, H. B. *Chemical Bonds: An Introduction to Atomic and Molecular Structure*; University Science Books: Mill Valley, CA 1994.

(2) (a) Strauss, S. H.; Silver, M. E.; Long, K. M.; Thomson, R. G.; Hudgens, R. A.; Spartalian, K.; Ibers, J. A. *J. Am. Chem. Soc.* **1985**, *107*, 4207–4215. (b) Goedken, V. L.; Pluth, J. J.; Peng, S.; Bursten, B. *J. Am. Chem. Soc.* **1976**, *98*, 8014–8021.
 (3) (a) Solomon, E. I.; Rawlings, J.; McMillin, J. R.; Stephens, P. J.; Gray, H. B. *J. Am. Chem. Soc.* **1976**, *98*, 8046–8048. (b) Bertini, I.; Luchinat, C. *Acc. Chem. Res.* **1983**, *16*, 272–279. (c) Bertini, I.; Lanini, G.; Luchinat, C. *J. Am. Chem. Soc.* **1983**, *105*, 5116–5118. (d) Khalifah, R. G.; Rogers, J. I.; Harmon, P. J.; Carroll, S. B. *Biochemistry* **1984**, *23*, 3129–3136. (e) Briganti, F.; Pierattelli, R.; Scozzafava, A.; Supuran, C. T. *Eur. J. Med. Chem.* **1996**, *31*, 1001–1010.
 (4) Maret, W.; Vallee, B. L. Cobalt as Probe and Label of Proteins. In *Methods Enzymol.* **1993**, *226*, 52–71.
 (5) (a) Lippard, S. J.; Berg, J. M. *Principles of Bioinorganic Chemistry*; University Science Books: Mill Valley, CA 1994; Chapter 12. (b) Bren, K. L.; Pecoraro, V. L.; Gray, H. B. *Inorg. Chem.* **2004**, *43*, 7894–7896.

coordination numbers encountered for this ion are four through six. Six-coordinate pseudooctahedral species typically populate high-spin configurations, although several low-spin systems under the influence of unusually strong ligand fields have been characterized.⁷ A host of six-coordinate systems also exhibit spin-crossover phenomena in the solid state.⁸ Sandwich and mixed-sandwich complexes (e.g., Cp₂Co, CpCoL₃⁺, TpCoCp; Tp = tris(pyrazolyl)borate) constitute a spectroscopically and magnetically rich subset of the octahedral Co(II) family.⁹ Five-coordinate Co²⁺ ions exhibit both trigonal bipyramidal and square pyramidal limiting structures. In contrast to the octahedral systems, these five-coordinate ions are most commonly low spin,¹⁰ although again both spin forms are well documented, as are systems that exhibit spin crossover in the solid state.^{11,12} Four-coordinate Co(II) systems are nominally either pseudo-tetrahedral or square planar, although a great many species are known to adopt structures that are highly distorted from these limiting structure types.¹³ Nevertheless, prior to recent studies undertaken by our laboratory^{14–16} all of the four-coordinate cobalt(II) systems that were known to exhibit low-spin ground-state configurations were classified as square planar. Ions of approximate tetrahedral geometries, whether nearly perfect *T_d* symmetry (e.g., CoCl₄²⁻) or species better described as pseudo-tetrahedral, distorted tetrahedral, or trigonal pyramidal had been without exception classified as high spin.^{17–20}

Our group has been exploring the nature of highly covalent pseudotetrahedral first-row transition ions (L₃M–X) supported by relatively strong field tris(phosphino)borate ligands ([BP₃]M–

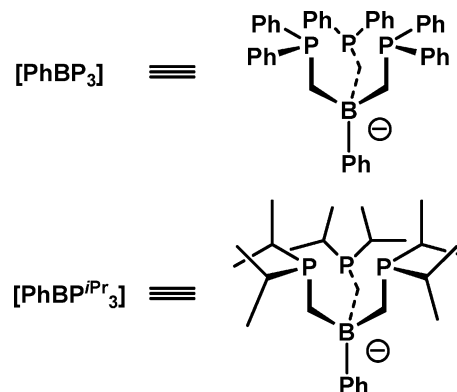


Figure 1. Chemical structures of [PhBP₃] and [PhBPⁱPr₃].

X). [BP₃] is the generic abbreviation used to denote these anionic tris(phosphino)borate ligands, and [PhBP₃] and [PhBPⁱPr₃] designate the [PhB(CH₂PPh₂)₃]⁻ and [PhB(CH₂PⁱPr₂)₃]⁻ anions, respectively (Figure 1). These [BP₃]M–X systems are striking in their propensity to populate low-spin electronic configurations. For example, we have characterized a series of L₃Fe–N_x species that can accommodate low-spin ground-state configurations for cases where (i) the iron center is either di-,²¹ tri-,^{22,23} or tetravalent²⁴ (i.e. d⁶, d⁵ or d⁴), and (ii) a favorable interaction exists with the N_x-type ligand that is characterized by one σ and two π bonds (e.g. *S* = 0, {[PhBP₃]Fe^{II}≡NR}⁻;²¹ *S* = 1/2, [BP₃]Fe^{III}≡NR;^{22,23} *S* = 0, [PhBPⁱPr₃]Fe≡N).²⁴ When the degree of π-bonding is attenuated, as is the situation for the divalent halides [BP₃]Fe–X,^{22,25} amides [PhBP₃]Fe–NRR',²⁶ alkyls [PhBPⁱPr₃]Fe–R,²⁷ and diazenidos [PhBPⁱPr₃]Fe–N=NR,²³ rigorously high-spin (*S* = 2) ground states are invariably populated.

By contrast, several divalent cobalt ions supported by these [BP₃] platforms populate low-spin (*S* = 1/2) ground-state electronic configurations, even in the absence of a strongly π-bonding X ligand. For example, we have reported that in solution the simple halides [PhBP₃]CoX (X = I, Br, Cl) each exhibit a doublet ground state that is predominantly populated at room temperature.^{14,15} The observed ground spin states of these complexes contrasts not only the numerous tetrahedral and distorted tetrahedral complexes studied previously but also tripodal borate Co(II) systems that are structurally very similar. These systems include Theopold's²⁸ and Moro-oka's²⁹ *S* = 3/2 [Tp''CoX] ([Tp''] = hydrotris(3-isopropyl-5-methylpyrazolyl)-borate species and Riordan's³⁰ *S* = 3/2 [PhTt^{tert-butyl}]CoX ([PhTt^{tert-butyl}] = PhB(CH₂SⁱBu)₃) derivatives.

- (6) (a) Lever, A. B. P. *Inorganic Electronic Spectroscopy*, 2nd ed.; Elsevier: New York, 1984; pp 480–505. (b) Cotton, F. A.; Wilkinson, G. *Advanced Inorganic Chemistry*, 5th ed.; Wiley: New York, 1988; p 729.
- (7) For examples of low-spin Co(II) octahedral systems see: (a) Faus, J.; Julve, M.; Lloret, F.; Muñoz, M. C. *Inorg. Chem.* **1993**, *32*, 2013–2017. (b) Santra, B. K.; Lahiri, G. K. *J. Chem. Soc., Dalton Trans.* **1998**, 139–145. (c) Iwatsuki, S.; Obeyama, K.; Koshino, N.; Funahashi, S.; Kashiwabara, K.; Suzuki, T.; Takagi, H. D. *Can. J. Chem.* **2001**, *79*, 1344–1351. (d) Reinen, D.; Ozarowski, A.; Jakob, B.; Pebler, J.; Stratemeier, H.; Wiegardt, K.; Tolksdorf, I. *Inorg. Chem.* **1987**, *26*, 4010–4017.
- (8) (a) Zarembowitch, J. *New J. Chem.* **1992**, *16*, 255–267. (b) Juhász, G.; Hayami, S.; Inoue, K.; Maeda, Y. *Chem. Lett.* **2003**, *32*, 882–883. (c) Sieber, R.; Decurtins, S.; Stoeckli-Evans, H.; Wilson, C.; Yufit, D.; Howard, J. A. K.; Capelli, S. C.; Hauser, A. *Chem. Eur. J.* **2000**, *6*, 361–368. (d) Gaspar, A. B.; Muñoz, M. C.; Niel, V.; Real, J. A. *Inorg. Chem.* **2001**, *40*, 9–10. (e) Faus, J.; Julve, M.; Lloret, F.; Real, J. A.; Sletten, J. *Inorg. Chem.* **1994**, *33*, 5535–5540. (f) Kremer, S.; Henke, W.; Reinen, D. *Inorg. Chem.* **1982**, *21*, 3013–3022.
- (9) For Cp₂Co see: (a) Gordon, K. R.; Warren, K. D. *Inorg. Chem.* **1978**, *17*, 987–994. (b) König, E.; Schnakig, R.; Kremer, S.; Kanellakopoulos, B.; Klenze, R. *Chem. Phys.* **1978**, *27*, 331–344. (c) Warren, K. D. *Struct. Bonding* **1976**, *27*, 45–159. For mixed sandwich complexes see: (d) Brunker, T. J.; Barlow, S.; O'Hare, D. *Chem. Commun.* **2001**, 2052–2053. (e) Brunker, T. J.; Crowley, A. R.; O'Hare, D. *Organometallics* **2002**, *21*, 3123–3138. (f) Brunker, T. J.; Green, J. C.; O'Hare, D. *Inorg. Chem.* **2003**, *42*, 4366–4381.
- (10) (a) Sacconi, L. *Coord. Chem. Rev.* **1972**, *8*, 351–367. (b) Morassi, R.; Bertini, I.; Sacconi, L. *Coord. Chem. Rev.* **1973**, *11*, 343–402.
- (11) (a) Kennedy, B. J.; Murray, K. S. *Inorg. Chim. Acta* **1987**, *134*, 249–254. (b) Kennedy, B. J.; Fallon, G. D.; Gatehouse, B. M. K. C.; Murray, K. S. *Inorg. Chem.* **1984**, *23*, 580–588.
- (12) (a) Thuéry, P.; Zarembowitch, J. *Inorg. Chem.* **1986**, *25*, 2001–2008. (b) Zarembowitch, J.; Kahn, O. *Inorg. Chem.* **1984**, *23*, 589–593.
- (13) Cirera, J.; Alemany, P.; Alvarez, S. *Chem. Eur. J.* **2004**, *10*, 190–207.
- (14) Shapiro, I. R.; Jenkins, D. M.; Thomas, J. C.; Day, M. W.; Peters, J. C. *Chem. Commun.* **2001**, 2152–2153.
- (15) Jenkins, D. M.; Di Bilio, A. J.; Allen, M. J.; Betley, T. A.; Peters, J. C. *J. Am. Chem. Soc.* **2002**, *124*, 15336–15350.
- (16) Jenkins, D. M.; Peters, J. C. *J. Am. Chem. Soc.* **2003**, *125*, 11162–11163.
- (17) (a) Ray, M.; Hammes, B. S.; Yap, G. P. A.; Rheingold, A. L.; Borovik, A. S. *Inorg. Chem.* **1998**, *37*, 1527–1532. (b) Sacconi, L.; Orlandini, A.; Midollini, S. *Inorg. Chem.* **1974**, *13*, 2850–2859. (c) Mani, F.; Mealli, C. *Inorg. Chim. Acta* **1981**, *54*, L77–L79.
- (18) Holm, R. H. *Acc. Chem. Res.* **1969**, *2*, 307–316.
- (19) Jaynes, B. S.; Doerr, L. H.; Liu, S.; Lippard, S. J. *Inorg. Chem.* **1995**, *34*, 5735–5744.
- (20) (a) Everett, G. W.; Holm, R. H. *J. Am. Chem. Soc.* **1965**, *87*, 5266–5267. (b) Cotton, F. A.; Soderberg, R. H. *J. Am. Chem. Soc.* **1962**, *84*, 872–873.

- (21) The complex {[PhBP₃]Fe≡N(1-Ad)}{NBu₄} has been thoroughly characterized (including by XRD analysis) and features a singlet ground state. Brown, S. D.; Peters, J. C. *J. Am. Chem. Soc.* **2005**, *127*, 1913–1923.
- (22) Brown, S. D.; Betley, T. A.; Peters, J. C. *J. Am. Chem. Soc.* **2003**, *125*, 322–323.
- (23) Betley, T. A.; Peters, J. C. *J. Am. Chem. Soc.* **2003**, *125*, 10782–10783.
- (24) Betley, T. A.; Peters, J. C. *J. Am. Chem. Soc.* **2004**, *126*, 6252–6254.
- (25) Betley, T. A.; Peters, J. C. *Inorg. Chem.* **2003**, *43*, 5074–5084.
- (26) Brown, S. D.; Peters, J. C. *J. Am. Chem. Soc.* **2004**, *126*, 4538–4539.
- (27) Daida, E. J.; Peters, J. C. *Inorg. Chem.* **2004**, *43*, 7474–7485.
- (28) (a) Reinaud, O. M.; Rheingold, A. L.; Theopold, K. H. *Inorg. Chem.* **1994**, *33*, 2306–2308. (b) Detrich, J. L.; Konečný, R.; Vetter, W. M.; Doren, D.; Rheingold, A. L.; Theopold, K. H. *J. Am. Chem. Soc.* **1996**, *118*, 1703–1712. (c) Jewson, J. D.; Liable-Sands, L. M.; Yap, G. P. A.; Rheingold, A. L.; Theopold, K. H. *Organometallics* **1999**, *18*, 300–305.
- (29) (a) Shirasawa, N.; Akita, M.; Hikichi, S.; Moro-oka, Y. *Chem. Commun.* **1999**, 417–418. (b) Shirasawa, N.; Nguyen, T. T.; Hikichi, S.; Moro-oka, Y.; Akita, M. *Organometallics* **2001**, *20*, 3582–3598.
- (30) (a) Schebler, P. J.; Riordan, C. G.; Guzei, I. A.; Rheingold, A. L. *Inorg. Chem.* **1998**, *37*, 4754–4755. (b) Schebler, P. J.; Mandimutsira, B. S.; Riordan, C. G.; Liabile-Sands, L. M.; Incarvito, C. D.; Rheingold, A. L. *J. Am. Chem. Soc.* **2001**, *123*, 331–332.

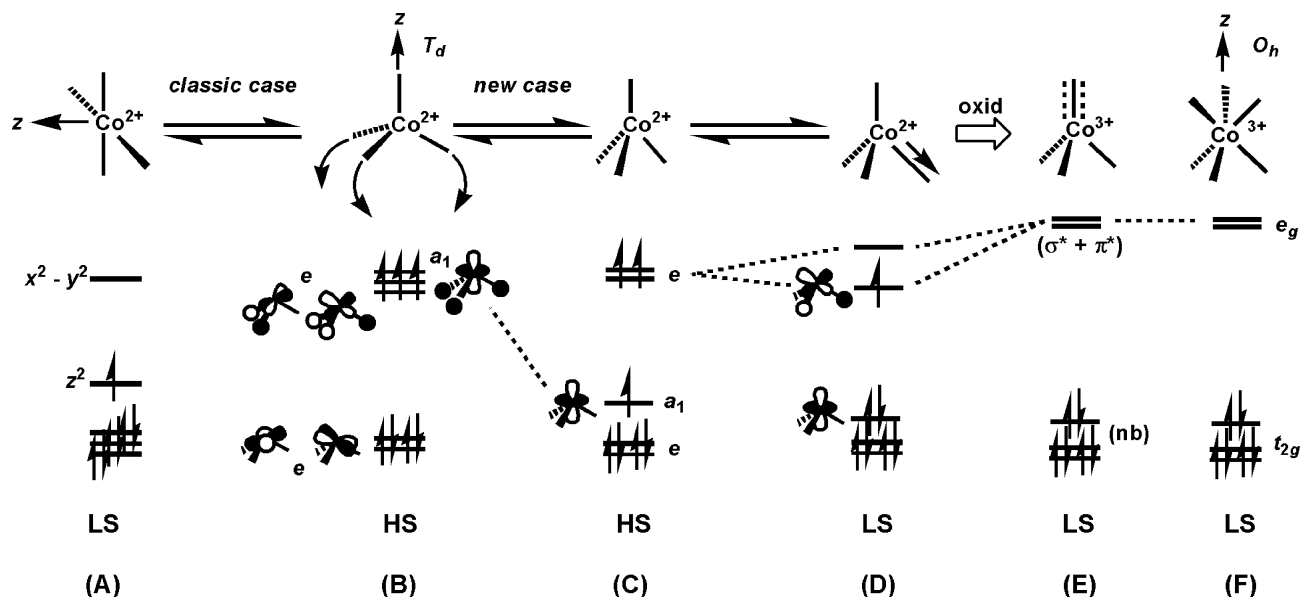


Figure 2. Qualitative stereochemical structures and d-orbital splitting diagrams relevant to the four-coordinate structures discussed in this report.

Several other puzzling observations have already been reported for the $[\text{BP}_3]\text{Co}^{\text{II}}-\text{X}$ family. For instance, a complex featuring an aryloxy X-type ligand, $[\text{PhBP}_3]\text{CoO}(2,6\text{-Me}_2\text{-Ph})$, exhibits a quartet rather than a doublet ground state.¹⁵ In addition, iodide and chloride complexes of the $[\text{PhBP}^{\text{iPr}}_3]$ anion ($[\text{PhBP}^{\text{iPr}}_3]\text{CoI}$ and $[\text{PhBP}^{\text{iPr}}_3]\text{CoCl}$) appear to populate rigorously high-spin ground states.²⁵ Each of these observations is somewhat counterintuitive. The $[\text{PhBP}^{\text{iPr}}_3]$ anion is more electron-releasing than $[\text{PhBP}_3]$,²⁵ and on the basis of electronic considerations its Co^{2+} complexes should be more likely to populate the low-spin configuration than $[\text{PhBP}_3]\text{Co}(\text{II})$ systems. The same is true of the aryloxy ligand. A more strongly π -donating aryloxy linkage might be expected to more favorably confer a low-spin ground-state configuration than a simple halide ligand.

Perceiving a need to broaden our appreciation of how the interplay between local stereochemistry, the L_3 donor ligand field strength, and the nature of the X-type ligand work to confer a specific electronic configuration, we set out to systematically characterize a host of pseudotetrahedral $[\text{BP}_3]\text{Co}-\text{X}$ ions amenable to structure/spin-state correlations. Herein we present the results of this study. Previous studies that have attempted to correlate steric factors with spin-state preferences have emphasized d^6 octahedral systems (e.g., $(\text{L}_3)_2\text{Fe}(\text{II})$).³¹ The systems described in this contribution afford a unique opportunity to examine spin-state preferences in *four-coordinate pseudotetrahedral L_3MX structures* by correlating an observed spin-state to the identity of a single X-type ligand, or the identity of an L_3 donor scaffold.

A qualitative sketch of the d-orbital splitting diagrams anticipated for the various limiting stereochemical structures is shown in Figure 2. Structures **A** and **B** illustrate the most familiar coordination geometries for four-coordinate Co^{2+} ions. These structure types are square planar (**A**) and tetrahedral (**B**) and give rise respectively to low-spin ($S = 1/2$) and high-spin

($S = 3/2$) ground-state configurations. An intramolecular distortion that interconverts **A** and **B** is denoted as the “classic case” in Figure 2. This phenomenon is well-known for $\text{Co}(\text{II})$ ions. Configurational and consequently spin-state equilibria in solution between $\text{Co}(\text{II})$ ions of these two limiting structure types is a phenomenon that was lucidly described by Holm and Everett nearly four decades ago.^{18,20a} Also, stereochemical tuning of $\text{Co}(\text{II})$ complexes using macrocyclic tetradentate ligands that can dictate one configuration versus another, and therefore different ground spin-states, was demonstrated by Lippard and co-workers using tropocoronand ligands.¹⁹

The interconversion between structures **A** and **B** is severe and is likely difficult to access in the crystalline state. A gentler distortion, denoted as the “new case” in Figure 2, is one of axial character and instead produces the pseudotetrahedral structure type **C**. Under three-fold symmetry (C_{3v}) a distortion of this type stabilizes an orbital of a_1 symmetry and provides a d-orbital splitting diagram comprised of $1a_1 + 2e$. This is a familiar orbital arrangement that has been frequently used to describe the electronic structures of sandwich (Cp^R_2M) and mixed-sandwich (Cp^RML_3) complexes.^{9,32} For sandwich complexes, the a_1 orbital is most typically placed slightly above a lowest-lying degenerate e-set, although the relative positioning of the lowest three orbitals ($a_1 + e$) has been debated.^{9c} An important point to underscore is that, to a first approximation, pseudotetrahedral complexes of structure type **C** (i.e. those typically supported by tripodal L_3 donor sets) are electronically best described using a crude “two-over-three” d-orbital splitting diagram akin to that of sandwich complexes such as Cp_2Fe . A tetrahedral splitting diagram is less appropriate. Therefore, while ligands that favor monomeric L_3MX structures are quite often referred to as “tetrahedral enforcers” owing to the pseudotetrahedral stereochemistry they confer, from an electronic structure perspective these ligands might be more appropriately regarded as “octahedral enforcers.” The tripodal ligand enforces the requisite axial distortion that gives rise to an approximate two-

(31) (a) Constable, E. C.; Baum, G.; Bill, E.; Dyson, R.; van Eldik, R.; Fenske, D.; Kaderli, S.; Morris, D.; Neubrand, A.; Neuburger, M.; Smith, D. R.; Wieghardt, K.; Zehnder, M.; Zuberbühler, A. D. *Chem. Eur. J.* **1999**, *5*, 498–508 and references therein. (b) Sohrin, Y.; Kokusen, H.; Matsui, M. *Inorg. Chem.* **1995**, *34*, 3928–3934.

(32) (a) Bally, T.; Borden, W. T. *Rev. Comput. Chem.* **1999**, *13*, 1–97. (b) Boone, A. J.; Chang, C. H.; Greene, S. N.; Herz, T.; Richards, N. G. J. *Coord. Chem. Rev.* **2003**, *238–239*, 291–314. (c) Carreón-Macedo, J.; Harvey, J. N. *J. Am. Chem. Soc.* **2004**, *126*, 5789–5797.

Table 1. Summary of Physical Properties

complex	color	Evans' method (μ_{eff} in BM, C ₆ D ₆ , 298 K)	SQUID $\chi_m T$ (cm ³ K mol ⁻¹) at 20 K, 300 K	Co ^{II} /Co ^{III} , Co/Co ^{II} (mV) ^a
[PhBP ₃]CoI, 1	green	2.8	0.82, 1.01	10, -920
[PhBP ₃]CoOSiPh ₃ , 2	purple	3.4	0.47, 1.45	-360, -1290
[PhBP ₃]CoO(4- <i>t</i> -Bu-Ph), 3	red-brown	3.4	0.90, 1.90	-390, -1330
[PhBP ₃]CoO(C ₆ F ₅), 4	olive green	3.8	1.32, 2.13 (at 240 K)	NA, NA
[PhBP ₃]CoSPh, 5	red	2.4	0.40, 0.49	-160, -1120
[PhBP ₃]CoS(2,6-Me ₂ -Ph), 6	red	2.3	0.50, 0.51	-170, -1100
[PhBP ₃]CoS(2,4,6- <i>i</i> -Pr ₃ -Ph), 7	red-brown	2.8	0.46, 0.63	-80, -1190
[PhBP ₃]CoS(2,4,6- <i>t</i> -Bu ₃ -Ph), 8	red	3.9	2.05, 2.21	-60, -1080
[PhBP ₃]CoSSiPh ₃ , 9	green	2.5	0.47, 0.44	-210 (irreversible), -1010
[PhBP ₃]CoOSi(4-NMe ₂ -Ph) ₃ , 10	red	3.5	0.46, 1.56	-360, -1300
[PhBP ₃]CoOSi(4-CF ₃ -Ph) ₃ , 11	blue	3.9	1.22, 1.95	-60 (irreversible), -1080
[PhBP ₃]CoOCPPh ₃ , 12	blue-green	3.8	2.08, 2.28	-300, -1310
[PhBP ^r Pr ₃]CoI, 13	green	4.1	1.83, 1.90	60, -1250
[PhBP ^r Pr ₃]CoOSiPh ₃ , 14	purple	4.3	2.19, 2.36	100 (irreversible), -1690
[PhBP ^r Pr ₃]CoSSiPh ₃ , 15	green	4.0	0.47, 1.23	-140 (irreversible), -1330
{[PhBP ₃]CoOSiPh ₃ }	green	diamagnetic	diamagnetic	oxidation product of 2
{B(3,5-(CF ₃) ₂ -Ph) ₄ }				
{16} {B(3,5-(CF ₃) ₂ -Ph) ₄ }				

^a Electrochemical data were collected in THF with a glassy carbon working electrode, platinum wire counter electrode, and Ag/AgNO₃ reference electrode. All measurements were reported versus an external standard of ferrocene. Either [TBA][PF₆] or [TBA][ClO₄] was used as the supporting electrolyte, as specified in the Experimental Section.

over-three splitting of the d-orbitals under idealized three-fold symmetry. Thus, the ground-state electronic structures of three-fold symmetric [Tp^r]Co^{II}-X complexes are appropriately assigned as ⁴A_{2g},^{28,29,33} but as discussed further below, these ground states bear a closer electronic relationship to high-spin octahedral complexes, such as [Tp]₂Co,³⁴ than to high-spin tetrahedral complexes, such as [Cs]₂[CoCl₄].³⁵ As will be shown, these general ideas help to account for the relative ease with which complexes of the high-spin structure type **C** can cross over to a related but low-spin structure type **D**, given appropriate choice of the donor ligand set.

II. Results and Discussion

Synthesis and Routine Solution Characterization of [BP₃]-Co^{II}-X Complexes. To more thoroughly examine structure/spin-state relationships within the [BP₃]Co^{II}-X system we prepared a series of [BP₃]Co^{II}-X complexes that feature O-atom and S-atom X-type linkages. Table 1 lists each of the [BP₃]Co complexes featured in the present study, along with their numerical designations (**1–16**) and standard magnetic and electrochemical characterization data. A fair number of alkoxide, aryloxy, thiolate, and arylthiolate derivatives of cobalt have been described previously, and several L₃MX systems that are structurally related to the present cobalt derivatives warrant specific mention. For instance, tris(pyrazolyl)borate (Tp) derivatives of cobalt(II)^{28,29,33} that feature X-type linkages related to the present systems have been reported. There are also several neutral tris(phosphine) Co(I) complexes, for example (PPh₃)₃-CoOPh,^{36,37} although we are unaware of any four-coordinate P₃Co^{II}X species other than those supported by [BP₃] ligands.

A tripodal amine donor ligand system that supports complexes with a single aryloxy ligand bound to cobalt has also been described.³⁸

The choice of [BP₃]Co^{II}-X complexes that feature O-atom and S-atom X-type linkages was due to the relative ease with which steric and electronic parameters could be tuned in a systematic fashion, and to the ease with which their Co(II) complexes could be generated and purified. Other X-type linkages were considered, for example alkyls and amides, but these types of complexes have proven to be synthetically problematic within the [BP₃]Co-X family. Attempts to prepare them has led to problematic side reactions indicative of undesirable redox chemistry rather than clean metalation.

The family of complexes shown in Table 1 is conveniently accessible via the use of soft thallium reagents TIEAr (eq 1). The typical method for preparation of these thallium reagents involves a metathesis reaction between commercially available thallium ethoxide and the desired phenol, arylthiol, silanol, or silylthiol.³⁹ The types of alcohols and thiols amenable to this method of preparation are restricted to those that have pK_a values lower than that of the ethanol byproduct (pK_a = 15.9). The addition of one equivalent of the desired thallium reagent as a THF solution to a THF solution of [BP₃]CoX (X = I or Cl) affords the substituted product in high crude yield with TlX as an easily separable byproduct. Filtration of the crude reaction mixture followed by crystallization, typically by vapor diffusion of petroleum ether in benzene, provides each of the desired complexes in crystalline form in modest to high yields (Table 1).



X = I or Cl;

ER = aryloxy, siloxide, thiolate, silylthiolate

Despite the paramagnetic nature of these Co(II) derivatives, ¹H NMR spectroscopy aids in their characterization. The

(33) (a) Thompson, J. S.; Sorrell, T.; Marks, T. J.; Ibers, J. A. *J. Am. Chem. Soc.* **1979**, *101*, 4193–4201. (b) Yoshimitsu, S.; Hikichi, S.; Akita, M. *Organometallics* **2002**, *21*, 3762–3773.

(34) (a) Jesson, J. P.; Trofimenko, S.; Eaton, D. R. *J. Am. Chem. Soc.* **1967**, *89*, 3148–3158. (b) De Alwis, D.; Chanaka, L.; Schultz, F. A. *Inorg. Chem.* **2003**, *42*, 3616–3622.

(35) (a) Katzin, L. I. *J. Am. Chem. Soc.* **1954**, *76*, 3089–3090. (b) Katzin, L. I.; Gebert, E. *J. Am. Chem. Soc.* **1953**, *75*, 2830–2832. (c) Schmidtko, H.; Nover, J. *Inorg. Chem. Acta* **1995**, *240*, 231–237.

(36) Hayashi, Y.; Yamamoto, T.; Yamamoto, A.; Komiya, S.; Kushi, Y. *J. Am. Chem. Soc.* **1986**, *108*, 385–391.

(37) (a) Kownacki, I.; Kubicki, M.; Marciniak, B. *Polyhedron* **2001**, *20*, 3015–3018. (b) Osakada, K.; Takizawa, T.; Tanaka, M.; Yamamoto, T. *J. Organomet. Chem.* **1994**, *473*, 359–369. (c) Tran, D. T. T.; Taylor, N. J.; Corrigan, J. F. *Angew. Chem., Int. Ed.* **2000**, *39*, 935–937.

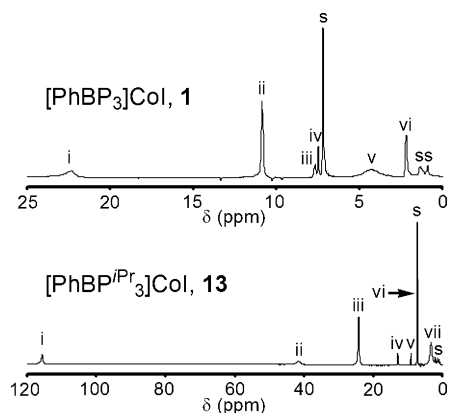


Figure 3. ^1H NMR spectra of **1** and **13** in C_6D_6 . Assignments are based on the correlation between single scan integration values and T_1 relaxation times for each resonance. For **1**: (i) $\text{PhB}(\text{CH}_2\text{PPh}_2)_3$, (ii) $m\text{-P}(\text{C}_6\text{H}_5)_2$, (iii) $o\text{-B}(\text{C}_6\text{H}_5)$, (iv) $m\text{-}$ and $p\text{-B}(\text{C}_6\text{H}_5)$, (v) $o\text{-P}(\text{C}_6\text{H}_5)_2$, (vi) $p\text{-P}(\text{C}_6\text{H}_5)_2$. For **13**: (i and ii) $\text{PhB}(\text{CH}_2\text{P}^i\text{Pr}_2)_3$ and $\text{P}(\text{CH}(\text{CH}_3)_2)_2$, (iii and vii) $\text{P}(\text{CH}(\text{CH}_3)_2)_2$, (iv) $o\text{-B}(\text{C}_6\text{H}_5)$, (v) $p\text{-B}(\text{C}_6\text{H}_5)$, (vi) $m\text{-B}(\text{C}_6\text{H}_5)$. s indicates a residual solvent resonance.

signature proton resonances are listed for each isolated complex in the Experimental Section. We examined the paramagnetically shifted ^1H NMR spectra of the iodides, $[\text{PhBP}_3]\text{CoI}$ (**1**) and $[\text{PhBP}^i\text{Pr}_3]\text{CoI}$ (**13**), in some detail as representative of this family of complexes. Both complexes exhibit solution spectra (see Figure 3) consistent with approximate C_3 symmetry at room temperature, as only a single set of resonances arises from the phosphine donor arms. T_1 relaxation times can be used as a guide to determine the relative distances of ligand-based protons from a coordinated metal center containing unpaired spin.⁴⁰ By measuring a T_1 relaxation time for each proton resonance shown in Figure 3 (top and bottom), and correlating these relaxation times with the integrated number of protons corresponding to each resonance, we are able to assign the spectrum of **1** with a high degree of confidence as indicated. The spectrum of **13** suffers from some ambiguity due to certain resonances having similar T_1 relaxation times and integration values. Notably, the chemical shift range of the resonances observed for **13** is much broader than that of **1**, likely due to their different respective spin states (vide infra).

Electrochemical Data. The electrochemical response of each complex featured in this study was examined by cyclic voltammetry in THF solution using either $[\text{Bu}_4\text{N}][\text{PF}_6]$ or $[\text{Bu}_4\text{N}][\text{ClO}_4]$ as the supporting electrolyte, a glassy carbon working electrode, a platinum wire counter electrode, and a Ag/AgNO_3 reference electrode. The potentials of well-defined redox processes were recorded versus an external ferrocene standard and are listed in Table 1.

The electrochemical data are generally unremarkable, but a few comparative comments are warranted. For those $[\text{PhBP}_3]\text{-Co(II)}$ complexes featuring a Co-OR linkage, specifically complexes **2**, **3**, **4**, **10**, **11**, and **12**, fully reversible Co(II/III) and Co(I/II) redox processes are observed. Relatively little shift in the potential of either redox event is apparent within this family, with the exception of the $p\text{-CF}_3$ -substituted silyloxyde

species $[\text{PhBP}_3]\text{CoOSi}(4\text{-CF}_3\text{-Ph})_3$ **11**. For this complex the Co(I/II) redox event is anodically shifted by ca. 300 mV, and the Co(II/III) redox event is irreversible. These differences are likely due to the electron-withdrawing CF_3 substituent, which destabilizes the higher-valent Co(III) state but renders the lower-valent Co(I) state more readily accessible.

The $[\text{PhBP}_3]\text{Co(II)}$ arylthiolate complexes **5–9** also exhibit well-behaved Co(II/III) and Co(I/II) redox events. These thiolate species are, as might be expected, easier to reduce and more difficult to oxidize than their aryloxy relatives. Again, only a small degree of variance is observed for the potentials among the arylthiolate family of complexes. Two subtle differences worth noting are that (i) complexes $[\text{PhBP}_3]\text{CoS}(2,4,6\text{-}^i\text{Pr}_3\text{-Ph})$, **7**, and $[\text{PhBP}_3]\text{CoS}(2,4,6\text{-}^t\text{Bu-Ph})$, **8**, are approximately 100 mV more difficult to oxidize than $[\text{PhBP}_3]\text{CoSPh}$, **5**, and $[\text{PhBP}_3]\text{-CoS}(2,6\text{-Me}_2\text{-Ph})$, **6**, presumably reflecting the difference in electron-releasing character between the arylthiolate substituents and (ii) it is ca. 100 mV more difficult to reduce **7** than **8**, an observation that is difficult to rationalize in simple terms. The triphenylsilylthiolato derivative $[\text{PhBP}_3]\text{CoSSiPh}_3$ (**9**) is the most easily reduced species (-1010 mV) but displays an irreversible oxidation event around -210 mV. The reduction potential recorded for complex **9** can be compared with that of its $[\text{PhBP}^i\text{Pr}_3]$ -supported congener $[\text{PhBP}^i\text{Pr}_3]\text{CoSSiPh}_3$ (**15**). The latter complex **15** is ca. 300 mV more difficult to reduce (-1330 mV) due to its more electron-releasing P_3 donor scaffold, but still displays an irreversible Co(II/III) process. Comparison of the redox processes observed between $[\text{PhBP}_3]\text{CoOSiPh}_3$, **2**, and $[\text{PhBP}^i\text{Pr}_3]\text{CoOSiPh}_3$, **14**, reveals another curiosity of note. While **14** is appreciably more difficult to reduce (by ca. 400 mV), as should be expected, its oxidation to Co(III) is electrochemically irreversible. By contrast, $\{[\text{PhBP}_3]\text{Co}^{\text{III}}\text{-OSiPh}_3\}^+$ is electrochemically accessible and stable (vide infra). This is difficult to rationalize, except to suggest that a putative $\{[\text{PhBP}^i\text{Pr}_3]\text{Co}^{\text{III}}\text{OSiPh}_3\}^+$ species may be more prone to loss of the triphenylsilyl substituent in the presence of a fluorinated counteranion from the electrolyte.

Finally, it is interesting to compare the electrochemical data recorded for these cobalt systems with that of a related series of recently reported $[\text{BP}_3]\text{Ni-X}$ systems.⁴¹ For example, a reversible Ni(II/I) reduction event is observed for the complex $[\text{PhBP}_3]\text{NiOSiPh}_3$ at -1.47 V, which is ca. 180 mV more negative than the Co(II/I) event of **2**. More striking is how difficult it is to oxidize the nickel systems to the Ni(III) state. For the complex $[\text{PhBP}_3]\text{NiOSiPh}_3$, the first oxidative process is encountered at a potential that is ca. 700 mV more positive than for its cobalt analogue **2**. This large difference presumably reflects the relative instability of a d^7 versus a d^6 electronic configuration within the $[\text{BP}_3]\text{Ni-X}$ and $[\text{BP}_3]\text{Co-X}$ platforms, respectively.

Chemical Oxidation of **2 To Produce $\{[\text{PhBP}_3]\text{CoOSiPh}_3\}\text{-}\{\text{BAR}_4\}$, $\{\text{16}\}\{\text{BAR}_4\}$.** Reversible oxidation waves for these $[\text{BP}_3]\text{Co}^{\text{II}}\text{-X}$ derivatives suggest that their chemical oxidation might afford the corresponding trivalent $\{[\text{BP}_3]\text{Co}^{\text{III}}\text{-X}\}^+$ products, which would comprise a structurally unusual class of pseudotetrahedral Co(III) complexes (type **E** in Figure 2). We have prepared and thoroughly characterized one such example pertinent to the present study: $\{[\text{PhBP}_3]\text{CoOSiPh}_3\}\{\text{BAR}_4\}$,

(38) Archibald, S. J.; Foxon, S. P.; Freeman, J. D.; Hobson, J. E.; Pernutz, R. N.; Walton, P. H. *J. Chem. Soc., Dalton Trans.* **2002**, 2797–2799.

(39) The preparation was modified from this reference. See Experimental Section. Jazdzewski, B. A.; Holland, P. L.; Pink, M.; Young, V. G., Jr.; Spencer, D. J. E.; Tolman, W. B. *Inorg. Chem.* **2001**, *40*, 6097–6107.

(40) Ming, L. *Physical Methods in Bioinorganic Chemistry*; Que, L., Jr., Ed.; University Science Books: Sausalito, CA, 2000; pp 375–464.

(41) MacBeth, C. E.; Thomas, J. C.; Betley, T. A.; Peters, J. C. *Inorg. Chem.* **2004**, *43*, 4645–4662.

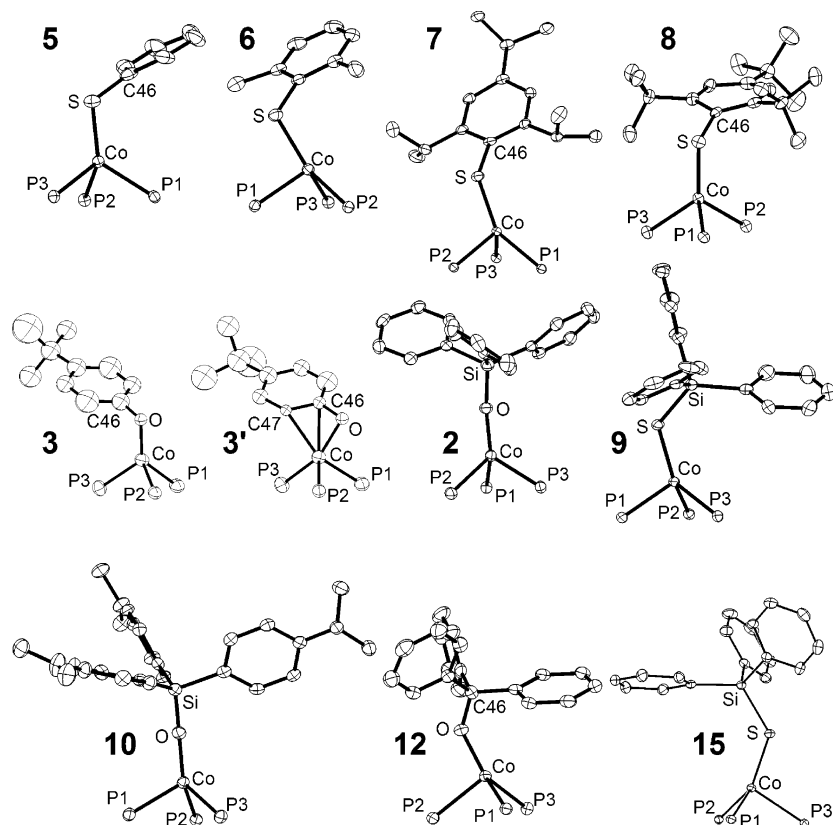
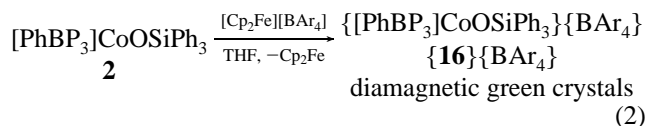


Figure 4. Displacement ellipsoid representations (50%) of the core structures of $[\text{PhBP}_3]\text{CoSPh}$ (**5**); $[\text{PhBP}_3]\text{CoS}(2,4,6\text{-}i\text{Pr}_3\text{-Ph})$ (**7**); $[\text{PhBP}_3]\text{CoS}(2,4,6\text{-}i\text{Pr}_3\text{-Ph})$ (**8**); $[\text{PhBP}_3]\text{CoO}(4\text{-}i\text{Bu-Ph})$ (**3**); $[\text{PhBP}_3]\text{CoOSiPh}_3$ (**2**); $[\text{PhBP}_3]\text{CoSSiPh}_3$ (**9**); $[\text{PhBP}_3]\text{CoOSi}(4\text{-NMe}_2\text{-Ph})_3$ (**10**); and $[\text{PhBP}_3]\text{CoOCPH}_3$ (**12**); $[\text{PhBP}^{i\text{Pr}}_3]\text{CoSSiPh}_3$ (**15**). The **3** and **3'** structures show the disorder in the $-\text{O}(4\text{-}i\text{Bu-Ph})$ ligand which is bound either η^1 (left) or η^3 (right) to the cobalt center. See Table 2 for bond lengths and angles, Table 3 for experimental parameters, and the Supporting Information for complete crystallographic details pertaining to each structure.

$\{\mathbf{16}\}\{\text{BAr}_4\}$ ($\text{Ar} = \text{C}_6\text{H}_5, 3,5\text{-(CF}_3)_2\text{-C}_6\text{H}_3$). The addition of THF to a solid mixture of **2** and $[\text{Cp}_2\text{Fe}][\text{BAr}_4]$ effects a rapid oxidation process to generate the diamagnetic, green product $\{\mathbf{16}\}\{\text{BAr}_4\}$ (eq 2). Cationic $\{\mathbf{16}\}\{\text{BAr}_4\}$ exhibits a sharp singlet in its ^{31}P NMR spectrum at 64.6 ppm and also a sharp singlet in the ^{19}F NMR spectrum at -58.5 for the tetra(3,5-bis(trifluoromethyl)phenyl)borate salt derivative. The combined ^1H and ^{31}P NMR spectra obtained for this system reveal that it is three-fold symmetric in solution on the NMR time scale. The diamagnetic ground state of $\{\mathbf{16}\}^+$ suggests that its electronic configuration is likely related to the diamagnetic imide $[\text{PhBP}_3]\text{Co}\equiv\text{N-}p\text{-tolyl}$, which is an $S = 0$ Co(III) species featuring a bona fide Co-N triple bond linkage.⁴² However, whereas $\{\mathbf{16}\}^+$ can be reduced at a potential of ca. -360 mV, the imide species $[\text{PhBP}_3]\text{Co}\equiv\text{N-}p\text{-tolyl}$ is stable to reduction at potentials as low as ca. -3.0 V, reflecting both the difference in charge and the weaker strength of the π -bonding in $\{\mathbf{16}\}^+$.



$$\text{Ar} = \text{Ph or } 3,5\text{-(CF}_3)_2\text{-C}_6\text{H}_3$$

Structural Characterization and Stereochemical Classification of $[\text{BP}_3]\text{Co}^{\text{II}}-\text{X}$ Derivatives. Solid-state crystal

(42) Jenkins, D. M.; Betley, T. A.; Peters, J. C. *J. Am. Chem. Soc.* **2002**, *124*, 11238–11239.

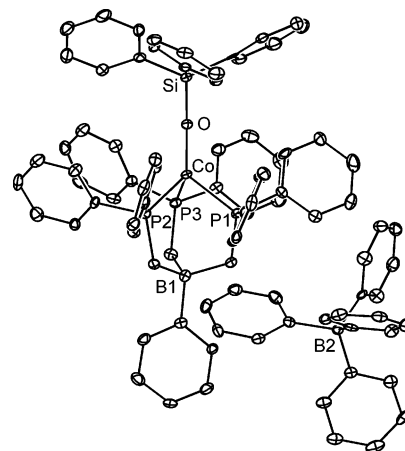


Figure 5. Displacement ellipsoid representations (50%) of $\{[\text{PhBP}_3]\text{CoOSiPh}_3\}\{\text{BPh}_4\}$, $\{\mathbf{16}\}\{\text{BPh}_4\}$. Hydrogen atoms and solvent molecules have been omitted for clarity. See Table 2 for bond lengths and angles, Table 3 for experimental parameters, and the Supporting Information for details.

structures have been determined for many of the cobalt complexes listed in Table 1. These results are summarized by their core structure representations, collected in Figures 4 and 5, and by a list of salient bond distances and angles, collected in Table 2. Table 3 lists pertinent crystallographic information. In each structure, the tris(phosphino)borate is κ^3 -bound to a monomeric cobalt center. The pseudotetrahedral structures can be broadly divided into two separate classes based on the average length of the Co-P bonds. As will be corroborated by

Table 2. X-ray Diffraction Table Showing Key Bond Lengths (Å) and Angles (deg) for **2**, **3**, **5**, **6**, **7**, **8**, **9**, **10**, **12**, **15**, and **{16}**{BPh₄}

	Co–E ^a	E–Z ^b	Co–P1	Co–P2	Co–P3	Co–E–X	P1–Co–P2	P1–Co–P3	P2–Co–P3	P1–Co–E	P2–Co–E	P3–Co–E
[PhBP ₃]CoOSiPh ₃ , 2	1.799(2)	1.612(2)	2.156(1)	2.284(1)	2.169(1)	172.5(1)	91.38(3)	85.88(3)	94.60(3)	129.45(7)	119.42(7)	125.82(7)
[PhBP ₃]CoO(4- ^t Bu-Ph), 3^c	1.832(7)	1.327(8)	2.247(1)	2.230(1)	2.227(1)	110.3(4)	91.48(4)	90.96(4)	96.35(4)	133.4(3)	106.9(2)	127.5(3)
[PhBP ₃]CoO(4- ^t Bu-Ph), 3^c	1.885(4)	1.330(6)	2.247(1)	2.230(1)	2.227(1)	88.4(3)	91.48(4)	90.96(4)	96.35(4)	97.6(2)	110.8(1)	151.2(1)
[PhBP ₃]CoSPh, 5^d	2.153(1)	1.742(4)	2.175(1)	2.178(1)	2.249(1)	104.3(1)	89.44(4)	97.52(4)	90.70(4)	121.14(4)	143.46(4)	103.24(4)
[PhBP ₃]CoS(2,6-Me ₂ -Ph), 6	2.167(1)	1.781(2)	2.251(1)	2.199(1)	2.208(1)	114.6(1)	89.44(2)	100.23(2)	86.73(2)	96.48(2)	147.37(2)	123.30(2)
[PhBP ₃]CoS(2,4,6- ⁱ Pr ₃ -Ph), 7^d	2.155(1)	1.802(2)	2.201(1)	2.280(1)	2.205(1)	123.2(1)	89.26(2)	88.14(2)	98.04(2)	143.37(2)	107.92(2)	119.75(2)
[PhBP ₃]CoS(2,4,6- ^t Bu ₃ -Ph) 8	2.207(1)	1.784(5)	2.354(1)	2.351(1)	2.387(1)	111.3(2)	96.11(5)	92.81(5)	96.30(5)	109.46(5)	125.24(5)	128.37(6)
[PhBP ₃]CoSSiPh ₃ , 9	2.190(1)	2.120(1)	2.206(1)	2.167(1)	2.243(1)	128.0(1)	87.79(3)	99.63(3)	87.65(3)	108.15(3)	139.91(3)	123.62(3)
[PhBP ₃]CoOSi(4-NMe ₂ -Ph) ₃ , 10	1.809(1)	1.618(2)	2.265(1)	2.144(1)	2.194(1)	165.7(1)	90.43(2)	94.56(2)	86.47(2)	117.36(5)	127.61(5)	129.77(5)
[PhBP ₃]CoOCPh ₃ , 12^d	1.839(1)	1.398(2)	2.349(1)	2.361(1)	2.387(1)	138.0(1)	92.56(2)	95.67(2)	92.40(2)	126.83(5)	102.99(5)	133.18(5)
[PhBP ₃]CoSSiPh ₃ , 15	2.178(1)	2.113(1)	2.179(1)	2.179(1)	2.357(1)	131.5(1)	90.30(2)	92.75(2)	93.27(2)	136.69(2)	126.30(2)	105.64(2)
{[PhBP ₃]CoOSiPh ₃ }{BPh ₄ }, {16}	1.766(3)	1.652(3)	2.187(1)	2.182(1)	2.184(1)	178.6(2)	90.67(5)	90.18(5)	90.50(5)	125.6(1)	124.4(1)	124.8(1)

^a E represents the fourth, non-phosphine atom directly bound to the Co center, either O or S. ^b Z represents the non-cobalt atom bound to E, either C or Si. ^c This complex features an aryloxide ligand distorted over two positions. **3** shows the bond distances and angles for the η^1 conformation. **3'** shows the bond angles and distances for the η^3 conformation. ^d There are two crystallographically independent molecules in the unit cell. Structural parameters for the nearly isomorphous second structure can be found in the Supporting Information.

the SQUID and EPR data discussed below, complexes featuring average Co–P bond distances between 2.15 and 2.25 Å (e.g., **6** and **10**) are characteristic of low-spin ground states (type **D** in Figure 2), whereas those with average Co–P bond distances between 2.30 and 2.35 Å (e.g., **8** and **12**) are characteristic of high-spin ground states (type **C** in Figure 2).

The basic stereochemical structures observed in the solid state can be further classified, at least qualitatively, as having one of two general structure types that we will refer to throughout as either umbrella distorted or off-axis distorted (Figure 6).¹³ In the former limiting description, the X-type ligand is regarded as axial and trisects the three Co–P linkages, coincident with the B–Co vector. In the latter limiting description the X-type ligand cants away from the imaginary vector running through the B and Co atoms to such an appreciable extent that it is better regarded as an equatorial ligand rather than an axial ligand. Distortions of an umbrella type are common for four-coordinate complexes supported by tripodal ligands, and it may be said that such ligands in fact enforce the umbrella distortion.^{28,30} Four-coordinate complexes that exhibit an off-axis distortion are less frequently encountered and appear to arise from the population of a low-spin ground state, as discussed in greater detail below.

Rigorously distinguishing between structures that arise from these two limiting distortions is not readily apparent by inspection. An elegant method known as the *continuous symmetry measure*^{13,43} proves very useful in this regard because it allows one to quantitatively discuss how close a given molecular geometry is to an idealized structure type. For example, Alvarez and co-workers have used this approach to quantitatively compare observed geometric structures to those of idealized tetrahedra or square planes.¹³ Under a continuous symmetry measurement, the distance (i.e., deviation) of a given molecule from an idealized polyhedron of a symmetry point group defined as *G* is numerically defined as *S*(*G*). A perfect

tetrahedron therefore has an *S*(*T_d*) = 0, and a perfect square plane has an *S*(*D_{4h}*) = 0. Construction of a 2-D plot of *S*(*G*) values can then be used to show that a perfect tetrahedron has an *S*(*D_{4h}*) = 33.3, and a perfect square plane has an *S*(*T_d*) = 33.3.¹³ As should be obvious, a trigonal pyramidal structure is geometrically much closer to a tetrahedron than a square plane, and this is reflected by its respective *S*(*G*) values; it features a relatively small *S*(*T_d*) by comparison to a large *S*(*D_{4h}*) value (*S*(*T_d*) = 3.57; *S*(*D_{4h}*) = 34.87).

Plotting the data for the X-ray structures shown in Figures 4 and 5 on a 2-D continuous symmetry map allows us to see the deviations. Comparing the species on a *S*(*T_d*) versus *S*(*D_{4h}*) map shows that the complexes we have prepared are all reasonably close to an ideal tetrahedron (Figure 7). Complexes on the upper left portion of the graph exhibit a typical umbrella distortion and are high spin (vide infra). This class includes complexes [PhBP₃]CoS(2,4,6-^tBu₃-Ph) (**8**), [PhBP₃]CoOCPh₃ (**12**), and [PhBP^{Pr}₃]CoI (**13**). The ambient temperature solid-state structure of [PhBP₃]CoOSiPh₃ (**2**) is also in this class (see Supporting Information).¹⁶ The upper-right box features low-spin umbrella complexes including the siloxides **2** (98 K structure), [PhBP₃]CoOSi(4-NMe₂-Ph)₃ (**10**), and {[PhBP₃]CoOSiPh₃}{BPh₄} ({**16**}-{BPh₄}) and the iodide complex we previously reported, [PhBP₃]CoI (**1**).¹⁵ The complexes we denote as off-axis distorted structure types are somewhat distinct from the [PhBP₃]Co^{II}–X complexes we have described in previous studies (lower right box in Figure 7).^{14,15} These off-axis complexes all incorporate a thiolate as the fourth ligand. Furthermore, all of these off-axis distorted species (**5**, **6**, **7**, **9**, and **15**) are low spin at 98 K. These five complexes feature one elongated Co–P bond in an axial position and two shorter Co–P bonds in the equatorial positions.

Given that all of these P₃Co^{II}X species show a modest distortion from an ideal tetrahedron, it is worth examining whether some of the species are better described as trigonal pyramidal. A continuous symmetry plot mapping the deviations from an ideal trigonal pyramid and a tetrahedron is shown in Figure 8. Almost all of the complexes fall within the middle portion of the graph, implying roughly equal distortions from

(43) (a) Avnir, D.; Katzenelson, O.; Keinan, S.; Pinsky, M.; Pinto, Y.; Salomon, Y.; Zabrodsky, H. *Concepts in Chemistry: A Contemporary Challenge*; Rouvray, D. H., Ed.; Research Studies Press: Taunton (UK), 1996. (b) Alvarez, S.; Avnir, D.; Llunell, M.; Pinsky, M. *New J. Chem.* **2002**, *26*, 996–1009.

Table 3. Crystallographic Details for [PhBP₃]CoOSiPh₃ (**2**), [PhBP₃]CoO(4-Bu-Ph) (**3**), [PhBP₃]CoSPh (**5**), [PhBP₃]CoS(2,6-Me₂-Ph) (**6**), [PhBP₃]CoS(2,4,6-*i*-Pr₃-Ph) (**7**), [PhBP₃]CoS(2,4,6-*Bu*₃-Ph) (**8**), [PhBP₃]CoSSiPh₃ (**9**), [PhBP₃]CoOSi(4-NMe₂-Ph)₃ (**10**), [PhBP₃]CoOCPh₃ (**12**), [PhBP^{Pr}₃]CoSSiPh₃ (**15**), and {[PhBP₃]CoOSiPh₃}{BPh₄}, {**16**}{BPh₄}

	[PhBP ₃]CoOSiPh ₃ , (2)	[PhBP ₃]CoO(4-Bu-Ph), (3)	[PhBP ₃]CoSPh, (5)	[PhBP ₃]CoS(2,6-Me ₂ -Ph), (6)
chemical formula	C ₆₃ H ₅₆ BOP ₃ SiCo·1.5(C ₆ H ₆)	C ₅₅ H ₅₄ BCoOP ₃	C ₅₁ H ₄₁ BCoP ₃ S	C ₅₃ H ₅₀ BCoP ₃ S
formula weight	1136.98	893.63	853.59	881.64
<i>T</i> (K)	98	98	98	98
λ (Å)	0.71073	0.71073	0.71073	0.71073
<i>a</i> (Å)	13.1013(14)	38.2238(8)	16.8066(16)	12.0158(9)
<i>b</i> (Å)	14.4428(16)	38.2238(8)	14.0767(13)	12.5469(9)
<i>c</i> (Å)	16.9894(19)	12.4091(5)	19.2736(18)	15.5078(12)
α (deg)	77.984(2)	90	90	77.780(1)
β (deg)	67.962(1)	90	113.801(2)	77.546(1)
γ (deg)	89.536(2)	90	90	77.919(1)
<i>V</i> (Å ³)	2905.8(6)	18130.4(9)	4172.0(7)	2198.2(3)
space group	<i>P</i> 1	<i>I</i> ₁ / <i>a</i>	<i>P</i> 2 ₁	<i>P</i> 1
<i>Z</i>	2	16	4	2
<i>D</i> _{calcd} (g/cm ³)	1.299	1.310	1.359	1.332
μ (cm ⁻¹)	4.44	5.25	6.10	5.80
R1, wR2 (<i>I</i> > 2 σ (<i>I</i>)) ^a	0.0336, 0.0673	0.0560, 0.0808	0.0463, 0.0661	0.0405, 0.0743
	[PhBP ₃]CoS(2,4,6- <i>i</i> -Pr ₃ -Ph), (7)	[PhBP ₃]CoS(2,4,6- <i>Bu</i> ₃ -Ph), (8)	[PhBP ₃]CoSSiPh ₃ , (9)	[PhBP ₃]CoOSi(4-NMe ₂ -Ph) ₃ , (10)
chemical formula	C ₆₀ H ₆₄ BCoP ₃ S	C ₆₃ H ₇₀ BCoP ₃ S·C ₆ H ₆	C ₆₃ H ₅₆ BCoP ₃ SSi·2 C ₆ H ₆	C ₆₉ H ₇₁ BCoN ₃ OP ₃ Si
formula weight	979.82	1100.01	1192.09	1149.03
<i>T</i> (K)	98	98	98	98
λ (Å)	0.71073	0.71073	0.71073	0.71073
<i>a</i> (Å)	15.3738(11)	13.8333(10)	11.0416(8)	12.1092(11)
<i>b</i> (Å)	17.3171(13)	13.9539(10)	12.8426(9)	12.3919(11)
<i>c</i> (Å)	20.7953(15)	17.5922(13)	22.3975(15)	21.3227(19)
α (deg)	65.655(1)	99.145(1)	87.228(1)	80.696(2)
β (deg)	87.329(2)	106.587(1)	81.435(1)	75.993(2)
γ (deg)	88.642(2)	107.029(1)	73.024(1)	72.962(1)
<i>V</i> (Å ³)	5038.5(6)	3000.8(4)	3003.7(4)	2954.0(5)
space group	$\bar{1}$	$\bar{1}$	$\bar{1}$	$\bar{1}$
<i>Z</i>	4	2	2	2
<i>D</i> _{calcd} (g/cm ³)	1.292	1.217	1.318	1.292
μ (cm ⁻¹)	5.20	4.40	4.70	4.40
R1, wR2 (<i>I</i> > 2 σ (<i>I</i>)) ^a	0.0482, 0.0836	0.0663, 0.1133	0.0529, 0.0777	0.0485, 0.0712
	[PhBP ₃]CoOCPh ₃ , (12)	[PhBP ^{Pr} ₃]CoSSiPh ₃ , (15)	{[PhBP ₃]CoOSiPh ₃ }{BPh ₄ }, { 16 }{BPh ₄ }	
chemical formula	C ₆₄ H ₅₆ BCoOP ₃ ·C ₆ H ₆	C ₄₅ H ₆₈ BCoP ₃ SSi	C ₈₇ H ₇₆ B ₂ CoOP ₃ Si·11/2 CH ₂ Cl ₂	
formula weight	1081.85	831.79	1466.50	
<i>T</i> (K)	98	98	98	
λ (Å)	0.71073	0.71073	0.71073	
<i>a</i> (Å)	12.9420(10)	10.3161(4)	13.592(2)	
<i>b</i> (Å)	20.8485(15)	14.4678(6)	14.814(2)	
<i>c</i> (Å)	21.5457(16)	29.963(1)	19.251(3)	
α (deg)	77.529(1)	90	72.567(3)	
β (deg)	82.143(1)	90	87.945(3)	
γ (deg)	88.626(1)	90	82.565(2)	
<i>V</i> (Å ³)	5622.9(7)	4472.0(3)	3667.0(9)	
space group	<i>P</i> 1	<i>P</i> 2 ₁ 2 ₁ 2 ₁	<i>P</i> 1	
<i>Z</i>	4	4	2	
<i>D</i> _{calcd} (g/cm ³)	1.278	1.235	1.328	
μ (cm ⁻¹)	4.40	6.00	4.70	
R1, wR2 (<i>I</i> > 2 σ (<i>I</i>)) ^a	0.0457, 0.0867	0.0431, 0.0606	0.0643, 0.1156	

both idealized geometries. Complexes **2**, **10**, **13**, and {**16**}⁺ exhibit less distortion from a tetrahedron, whereas complex **6**, while distorted from both idealized geometries, is slightly closer

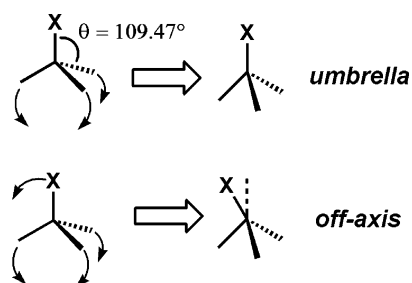


Figure 6. Limiting distortions relevant to the pseudotetrahedral structure types discussed in this report.

to a trigonal pyramid. It is admittedly difficult to tease out a definitive difference between these two ideal geometries for the structures described. The dotted line shown in Figure 8 qualitatively draws the same distinction illustrated by the previous graph (Figure 7). The complexes on the left side feature typical umbrella distortions and the complexes on the right feature off-axis distortions. The single discrepancy between this plot and the plot in Figure 7 is that this symmetry map suggests that complex **1** belongs to the off-axis class instead of the umbrella class. None of the complexes we have prepared is truly close to a trigonal pyramidal geometry since the equatorial L–Co–L angles are inequivalent. Known examples of trigonal pyramidal Co(II) species have been assigned as high spin and often feature a tetradentate ligand with three equivalent tripodal

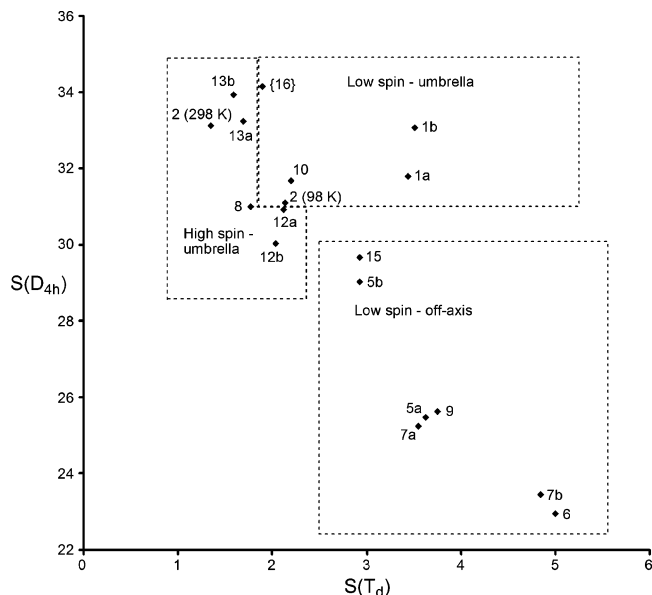


Figure 7. Calculated continuous symmetry deviation for each molecule is plotted on a continuous symmetry map of $S(T_d)$ (tetrahedral) versus $S(D_{4h})$ (square planar). The complexes can be assigned to one of two classes on the basis of their deviations from these two idealized structure types. The umbrella class can be subdivided into high-spin and low-spin complexes. Complexes with two components on the symmetry map (**a** and **b**) have two asymmetric molecules within the unit cell. The crystal structure of $[\text{PhBP}_3]\text{CoOSiPh}_3$ (**2**) was solved at two different temperatures.

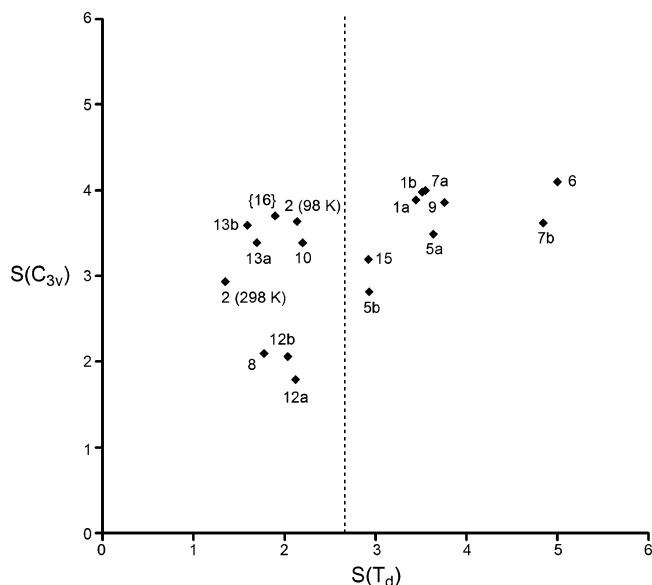


Figure 8. Calculated continuous symmetry deviation for each molecule is plotted on a continuous symmetry map of $S(T_d)$ (tetrahedral) versus $S(C_{3v})$ (trigonal pyramidal). Complexes to the left of the dashed line can be assigned as umbrella distorted, while those on the right can be assigned as off-axis distorted. Complexes with two components on the symmetry map (**a** and **b**) have two asymmetric molecules within the unit cell. The crystal structure of $[\text{PhBP}_3]\text{CoOSiPh}_3$ (**2**) was solved at two different temperatures.

arms and one axial donor ligand giving equivalent L–Co–L angles near 120° .¹⁷

Complex **3** does not follow the generalized descriptions discussed above since the aryloxide ligand is disordered over two positions, one that exhibits η^1 -bonding to the cobalt center (**3**) and one that displays η^3 -bonding (**3'**) (Figure 4).⁴⁴ To our

knowledge, an η^3 -binding mode of an aryloxide ligand is unprecedented for cobalt complexes. In the η^3 -bonding mode (**3'**), the Co–O bond distance is 1.885(4) Å and the Co–C bond distances are 2.277(5) and 2.341(5) for C(46) and C(47), respectively. Furthermore, the Co–O–C(46) bond angle is highly bent ($88.4(3)^\circ$) to accommodate favorable π -bonding to the aryl ring.

The solid-state structure determined for diamagnetic $\{\mathbf{16}\}$ - $\{\text{BPh}_4\}$ shows an umbrella distortion (Figure 5). The complex is markedly three-fold symmetric and represents an ideal example of structure type **E**, as shown in Figure 2. The Co–P distances display a variance of only 0.005 Å, and the average of the three Co–P distances is short at 2.185 Å (Table 2). The Co–O bond distance (1.766(3) Å) is only 0.03 Å shorter than in **2**, and the Co–O–Si bond angle is almost perfectly linear ($178.6(2)^\circ$). $[\text{PhBP}^{\text{Pr}_3}]\text{CoSSiPh}_3$ (**15**) features an off axis distortion. However, the axial elongation is much more pronounced for complex **15** than the other off axis complexes, and in this case, the axial Co–P bond is greater than 0.17 Å longer than the equatorial Co–P bonds.

Magnetic Characterization (SQUID and EPR) of $[\text{BP}_3]\text{Co}^{\text{II}}\text{--X}$ Derivatives. As mentioned in the Introduction, experimental evidence for the preferred low-spin ground-state configuration in a $\text{L}_3\text{Co}^{\text{II}}\text{--X}$ structure type was first provided by the complex $[\text{PhBP}_3]\text{CoI}$ (**1**).¹⁵ In the solid state this complex displays the distorted structure type represented as **D** in Figure 2. The related chloride and bromide complexes $[\text{PhBP}_3]\text{Co--X}$ are also low-spin species in their monomeric form in solution, but they give rise to dimeric structures in the crystalline state and are therefore of little utility to the present discussion. In contrast to these low-spin $[\text{PhBP}_3]\text{Co(II)}$ halides, we have previously assigned quartet ground states to the complexes $[\text{PhBP}^{\text{Pr}_3}]\text{CoI}$ (**13**), $[\text{PhBP}^{\text{Pr}_3}]\text{CoCl}$, and $[\text{PhBP}_3]\text{CoO}(2,6\text{-Me}_2\text{-Ph})$ (type **C** in Figure 2). These assignments, considered collectively, suggested to us the possibility that the low- and high-spin ground states of pseudotetrahedral $\text{L}_3\text{Co}^{\text{II}}\text{X}$ structure types may in fact lie closer in energy (i.e., $\Delta H_{\text{HS/Ls}} = k_{\text{B}}T$) than had been previously anticipated.^{15,25} For the collection of $[\text{PhBP}_3]\text{Co}^{\text{II}}\text{X}$ complexes presented in this paper (see Table 1) it is clear that a low-spin ground state is most typically, although not always, preferred. Moreover, this spin preference is in contrast to Co(II) species supported by the $[\text{PhBP}^{\text{Pr}_3}]$ ligand, where the high-spin configuration more typically dominates.

SQUID and EPR data have been collected for all of these $[\text{BP}_3]\text{Co(II)}$ complexes. Rigorously high-spin species include complexes **8**, **12**, **13**, and **14**. Each of these complexes adopts a structure that falls into the upper left portion of the symmetry plot shown in Figure 7, exhibiting a typical umbrella distortion. Complexes **1**, **5**, **6**, **7**, and **9** provide examples of rigorously low-spin species. The complexes **2**, **10**, **11**, and **15** display spin-crossover phenomena in the solid state. The low-spin Co(II) derivatives, type **D** in Figure 2, give rise to stereochemical structures exhibiting both umbrella and off-axis distortions. The interpretation of the magnetic data for **3** and **4** is more complex due to the potential for η^3 interactions from the X-type ligand.

In examining the $[\text{PhBP}_3]$ supported thiolates (**5–9**), it is apparent that the preferred ground state is ^2E . Each complex, excluding **8**, has values of $\chi_{\text{m}}T_{\text{av}}$ ($\text{cm}^3 \text{K mol}^{-1}$) from 10 to 300 K slightly above the spin only value of $\chi_{\text{m}}T = 0.375$ for a single unpaired electron: **5**, 0.41; **6**, 0.50; **7**, 0.51; **9**, 0.45 (see

(44) The atoms in the aryloxide ligand were refined isotropically. See Supporting Information for details.

Supporting Information for details). The solid-state magnetic moment of complexes **5** and **7** very gently increases as the temperature of each sample is raised above 250 K. We collected data from 4 to 300 K, and then back to 4 K for complex **7**, and this gentle curvature at higher temperatures was reproducible. It thus appears likely that partial population of an $S = 3/2$ state is present at higher temperatures. A similar curvature is also observed for [PhBP₃]CoI (**1**).¹⁵ Recall that the low-spin thiolates **5**, **6**, and **9** each exhibit an off-axis distortion in the solid-state and short average Co–P bond distances. The EPR data for these three species corroborates their doublet assignments, exhibiting axial ($g_{\parallel} > g_{\perp}$) EPR signals centered near $g = 2$ (see Supporting Information for details). On the other hand, complex **8** exhibits a $\chi_m T_{av}$ (10–300 K) value of 2.11 cm³ K mol⁻¹ between 10 and 300 K, an amount that is slightly greater than the spin only value for an $S = 3/2$ system (1.88 cm³ K mol⁻¹). Its low-temperature EPR spectrum confirms this assignment by showing two signals, one at $g \approx 2$ and a second signal at low field centered at $g \approx 5.8$. The $S = 3/2$ ground state of **8** must be due to high steric crowding by the bulky X-type thiolate ligand. Population of the quartet spin state expands the average Co–P bond distances, thereby alleviating unfavorable steric contacts.

Many pseudotetrahedral Co(II) complexes supported by [Tp] ligands have been prepared, and all of them are high spin.^{28,29} Given the preference we have found for [BP₃]Co-thiolates to populate low-spin ground states, we were curious as to whether a thiolate ligand might confer the low-spin configuration to a [Tp]Co(II) system. [Tp]Co thiolates have been prepared previously, and while magnetic data are not available for these species, they are presumed to be high spin.^{33a} We prepared one example of such a complex, [Tp^{3,5-Me2}]CoS(2,6-Me₂-Ph) (**17**), to obtain low-temperature magnetic and structural data for comparison with the [BP₃]CoX systems described herein. The X-ray structure for **17**, which is pseudotetrahedral, can be found in the Supporting Information. SQUID data for this sample unequivocally show that **17** populates a high-spin ground state, with χT_{av} (10–300 K) = 2.41 cm³ K mol⁻¹. The electronic distinction between [BP₃] and [Tp] ligands is thus evident.

Whereas thiolate ligands typically confer low-spin ground states in the case of [BP₃]Co(II) derivatives, weaker-field siloxide ligands form complexes that exhibit spin crossover, as evinced by the complexes [PhBP₃]CoOSiPh₃ (**2**), [PhBP₃]CoOSi(4-NMe₂-Ph)₃ (**10**), and [PhBP₃]CoOSi(4-CF₃-Ph)₃ (**11**). Each of these complexes exhibits an umbrella distortion at low temperature. The structure of **2** has been examined both at 98 K (see Figure 4) and at 298 K (see Supporting Information), and while the average of the Co–P bond distances is expanded at 298 K (reflecting population of the high-spin state, vide infra) both X-ray data sets confirm the umbrella distortion (Figure 7).¹⁶ Changing the substituents at the para position on the siloxide aryl rings dramatically effects the spin state population at a given temperature (Figure 9). The presence of the electron withdrawing CF₃ dramatically lowers the T_c of the spin crossover event. As shown in Figure 9, there is a strong temperature dependence of the moment of **10**, and a relatively well-defined partial hysteresis is evident centered around 150 K. A more gradual and fully reversible change in $\chi_m T$ is observed above 170 K. This magnetic behavior is distinct from the data collected for **2**, which shows gradual crossover (Figure 9). EPR spectra were collected at 20 K for **2**, **10**, and **11**, and the spectra are

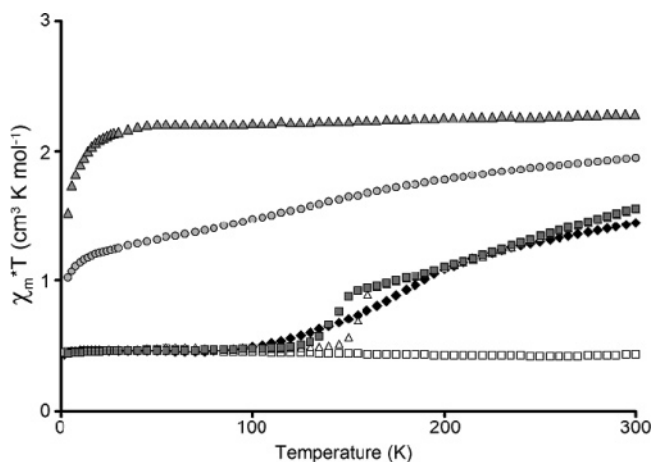


Figure 9. SQUID magnetization plot of $\chi_m T$ versus T : [PhBP₃]CoOSiPh₃ (**2**) (◆), [PhBP₃]CoOSi(4-CF₃-Ph)₃ (**11**) (●), [PhBP₃]CoOCPh₃ (**12**) (▲), [PhBP₃]CoSSiPh₃ (**9**) (□) [PhBP₃]CoOSi(4-NMe₂-Ph)₃ (**10**) as the temperature was raised (△) and lowered (■).

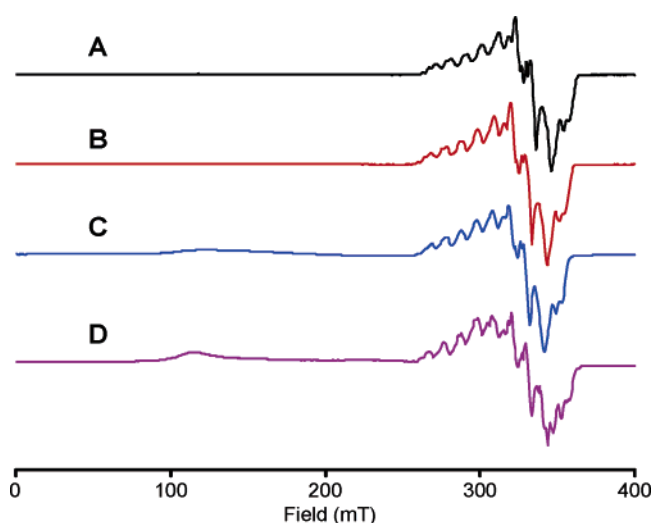


Figure 10. Glassy toluene EPR spectra (20 K) for (A) [PhBP₃]CoOSiPh₃ (**2**) (black line), (B) [PhBP₃]CoOSi(4-NMe₂-Ph)₃ (**10**) (red line), (C) [PhBP₃]CoOSi(4-CF₃-Ph)₃ (**11**) (blue line), (D) [PhBP₃]CoOCPh₃ (**12**) (purple line). Instrumental parameters for the spectra can be found in the Supporting Information.

consistent with the low-temperature SQUID data obtained for each sample.⁴⁵ The EPR spectrum of **2** shown in Figure 10A exhibits an axial signal ($g_1 = 2.21$, $g_2 = 2.05$, $g_3 = 2.03$) featuring well-defined hyperfine coupling ($I_{Co} = 7/2$) as well as superhyperfine coupling to phosphorus ($3 \times P$, $I_P = 1/2$). The observation of phosphorus coupling reflects the highly covalent character of these systems.⁴⁶ The octet pattern ($A_{1(Co)} = 105$ G) in the g_1 region of the spectrum confirms a monomeric species in solution in each case (see Supporting Information for simulated versus experimental spectra for **2**).¹⁶ Noticeably absent from the spectra of **2** and **10** are any low field signals that would signify the presence of a high-spin Co(II) component.⁴⁷ The EPR spectrum of **11** (Figure 10C) is more interesting. A broad but discernible signal at low field (near $g = 5.5$) is present at 20 K, suggesting the presence of a high-spin

(45) For a discussion of EPR of Co(II) see: Banci, L.; Bencini, A.; Benelli, C.; Gatteschi, D.; Zanchini, C. *Struct. Bonding* **1982**, *52*, 37–86.

(46) Stelzer, O.; Sheldrick, W. S.; Subramanian, J. *J. Chem. Soc., Dalton Trans.* **1976**, 966–970.

(47) Palmer, G. *Physical Methods in Bioinorganic Chemistry*; Que, L., Jr., Ed.; University Science Books: Sausalito, CA, 2000.

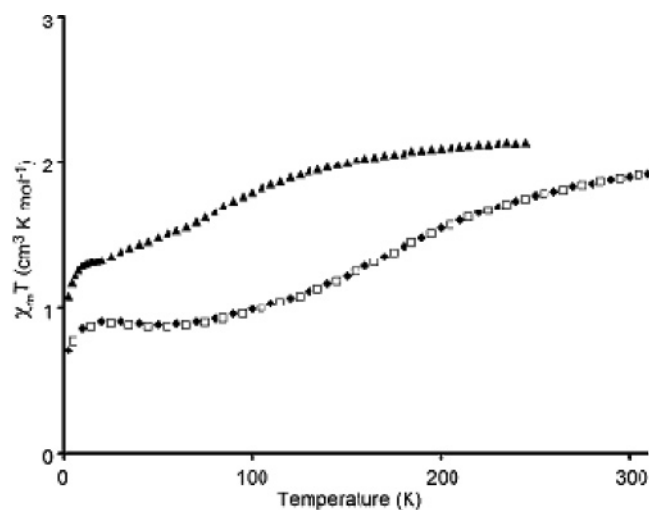


Figure 11. SQUID magnetization plot of $\chi_m T$ versus T for [PhBP₃]CoO(4-Bu-Ph) (**3**) as the temperature was raised (◆) and then lowered (□), and data for [PhBP₃]CoO(C₆F₅) (**4**) (▲) as temperature was raised.

component, as is also evident from the solid-state SQUID data. The hyperfine coupling in the $g = 2$ region of the spectrum can be attributed to the presence of the low-spin component of **11** in the glass, in analogy to the spectra of **2** and **10**. The effect of solvent in the crystal lattice on the spin-crossover process was measured for **2** in the solid state and was found to be minimal (see Supporting Information). Interestingly, the trityloxide complex [PhBP₃]CoOCPH₃ (**12**) exhibits a highly bent Co–O–C bond angle of 138.0(1)°, compared with the angle of 172.5(1)° for **2** and 165.7(1)° for related **10**. Moreover, each of the Co–P bond distances is expanded (Co–P_{av} = 2.37 Å), suggestive of a high-spin ground state in accord with its solid-state SQUID (Figure 9) and glassy toluene EPR data (Figure 10D). The disparate spin state preference between **2** and **12** underscores the electronic sensitivity of the [PhBP₃]Co system to modest modifications, even in the secondary coordination sphere.

The magnetic data are complicated for **3** and **4** by the possibility of η^3 interactions of the axial ligand. The solid-state crystal structure obtained for **3** at 98 K reveals the presence of two distinct conformational isomers. One of these isomers is a four-coordinate pseudotetrahedral species with a Co–O–C_{ipso} angle of 110.3(4)°. The other isomer is nominally five-coordinate and displays an η^3 -binding mode of the aryloxide ligand that provides an acute Co–O–C_{ipso} angle of 88.4(3)°. SQUID magnetization data for **3** are shown in Figure 11. It is clear that the sample predominantly populates a doublet state at low temperature, although a weak signal at low field is discernible in the glassy toluene EPR spectrum of the sample (see Supporting Information). As the sample is warmed the $\chi_m T$ value gradually rises and at 300 K almost complete crossover to the high-spin component is evident. Perhaps the simplest explanation of these data is that the pseudotetrahedral isomer of **3** is high spin at all temperatures, and that the isomer that exhibits an η^3 -bonding mode is low spin at all temperatures. The magnetic data would then reflect variable populations of the two conformational isomers as a function of temperature in both solid and solution. Consistent with this explanation is the fact that the two other pseudotetrahedral aryloxide and alkoxide complexes we have examined, [PhBP₃]CoO(2,6-Me₂-Ph)¹⁵ and [PhBP₃]CoOCPH₃ (**12**), both exhibit high-spin ground states,

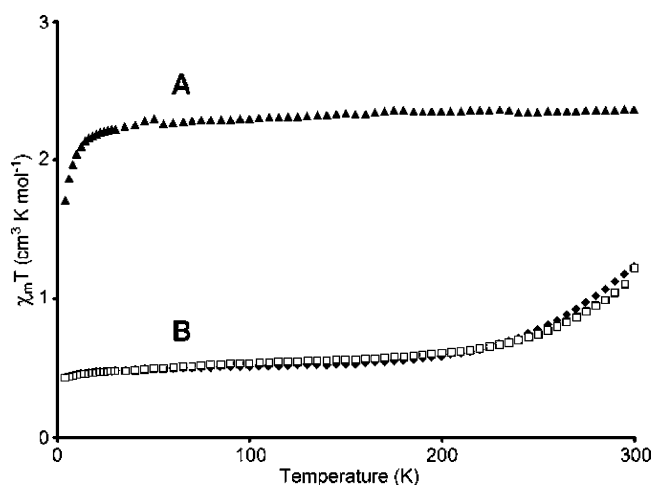


Figure 12. SQUID magnetization plot of $\chi_m T$ versus T for (A) [PhBPⁱPr₃]-CoOSiPh₃ (**14**) (▲), and (B) [PhBPⁱPr₃]CoSSiPh₃ (**15**) as temperature was raised (◆) and then lowered (□).

and the fact that five-coordinate cobalt(II) systems supported by phosphine ligands invariably populate low-spin ground states.¹⁰ The fluorinated aryloxide complex [PhBP₃]CoO(C₆F₅) (**4**) is less likely to exhibit π -bonding to the aryl ring due to its electron-withdrawing nature, although interactions with the ortho fluorines of the aryl group cannot be discounted. A similar four-coordinate/five-coordinate equilibrium may explain the change in spin state that is observed in the SQUID data (Figure 11).

The complexes supported by the [PhBPⁱPr₃] ligand feature two high-spin complexes, [PhBPⁱPr₃]CoI (**13**) and [PhBPⁱPr₃]-CoOSiPh₃ (**14**), that exhibit the umbrella distortion, and one thiolate complex, [PhBPⁱPr₃]CoSSiPh₃ (**15**), that exhibits an off-axis distortion and is low spin (vide infra) at low temperature. Structural and magnetic data have been reported previously for [PhBPⁱPr₃]CoI (**13**).²⁵ This complex exhibits a high-spin ground-state configuration and is therefore distinct from its low-spin analogue [PhBP₃]CoI (**1**).¹⁵ SQUID data collected on a polycrystalline sample of **14** are plotted in Figure 12A. The sample is clearly an $S = 3/2$ system ($\chi_m T_{av}$ (10 K – 300 K) = 2.30 cm³ K mol⁻¹) and obeys the Curie–Weiss law. Similar magnetic behavior was reported for iodide **13**.²⁵ Magnetization data for the thiolate derivative **15** are plotted in Figure 12B. The temperature dependence of its magnetic moment is more complex. Below 100 K the sample appears to be low spin ($\chi_m T_{av}$ (10 K – 100 K) = 0.50 cm³ K mol⁻¹). A gradual rise in $\chi_m T$ is observed above 100 K and a maximum value of 1.23 cm³ K mol⁻¹ is reached at 300 K, the highest temperature at which the data could be recorded. The magnetic behavior of the sample is fully reversible. The appearance of a gradual spin-crossover phenomenon is similar to the rise in magnetic moment that was observed for thiolates **5** and **7** near room temperature. An interesting observation is that the solution moment of **15** at room temperature is 4.0 μ_B , consistent with a fully high-spin population. This moment is different from that determined at low temperature by SQUID analysis of the polycrystalline sample, and we therefore elected to further analyze **15** by EPR spectroscopy as a powder and as a frozen glass. These data, along with the glassy toluene EPR spectrum of **14**, are shown in Figure 13. The 20 K glassy toluene spectra of **14** and **15** (Figure 13A and 13B) each show spectra characteristic of $S = 3/2$ species. The low field signal present in the glassy spectrum

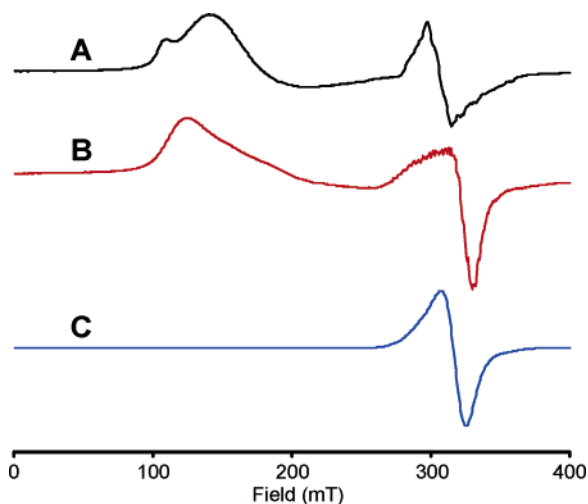


Figure 13. Glassy toluene EPR spectra (20 K) of (A) $[PhBP^{iPr_3}]CoOSiPh_3$ (**14**) (black line), and (B) $[PhBP^{iPr_3}]CoSSiPh_3$ (**15**) (red line). (C) Powder sample EPR spectrum (20 K) of $[PhBP^{iPr_3}]CoSSiPh_3$ (**15**) (blue line). Instrumental parameters for the spectra can be found in the Supporting Information.

of **15** is absent in its powder spectrum at 20 K (Figure 13C). There appears therefore to be a stronger preference to populate the high-spin configuration *in solution* for this thiolate complex. A different solution conformation of **15** may exist than the one that is observed in its solid-state structure at 98 K. Differences in spin behavior between solution and solid samples are not uncommon for spin-crossover systems.⁴⁸ Even with the stronger donor ligand $[PhBP^{iPr_3}]$ these complexes favor the high-spin state unless there is a fourth ligand that is an unusually strong donor such as a thiolate ligand. The extreme Co–P axial bond elongation in **15** likely reflects a steric compensation that allows the doublet ground state to be populated.

Theoretical Analysis of $[BP_3]Co^{II}-X$ Derivatives. To more thoroughly consider the case of their d^7 electronic structures we have undertaken the theoretical DFT examination of one representative complex from each structural subgroup. For this study we chose the siloxide complex $[PhBP_3]CoOSiPh_3$ (**2**) as representative of the umbrella subgroup, and thiolate $[PhBP_3]CoS(2,6-Me_2-Ph)$ (**6**) as representative of the off-axis subgroup. Single-point electronic structure calculations (DFT) were performed using (i) the experimentally determined X-ray coordinates for each complex as the ground-state geometrical structure under (ii) the assumption of a doublet electronic ground state. Each of the structures was subsequently allowed to relax into a theoretically determined global minimum in the absence of geometric constraints, but still under the assumption of a doublet ground-state electronic configuration. For each complex, the frontier molecular orbitals obtained by both methods of analysis are qualitatively quite similar. There are, however, noteworthy structural differences between the experimentally and theoretically determined structures.

For pseudotetrahedral **2** the predicted frontier molecular orbitals from the geometry-restricted calculation are shown in Figure 14. Orbitals calculated for the DFT-optimized structure are provided in the Supporting Information. The singly occupied molecular orbital (SOMO) is energetically well-separated from the lowest unoccupied orbital (LUMO). The lobal representa-

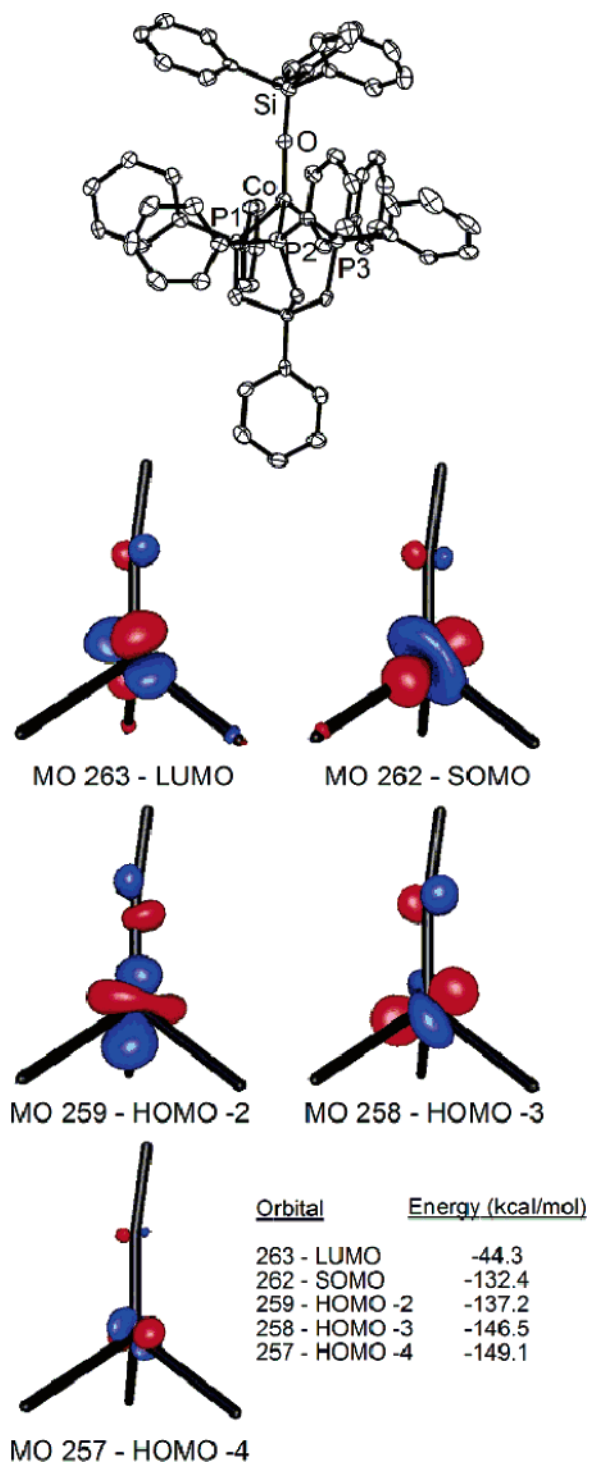


Figure 14. Molecular orbitals derived from a single-point energy DFT calculation of $[PhBP_3]CoOSiPh_3$ (**2**) assuming a doublet ground state and the crystallographically determined atomic coordinates. The DFT minimized structure of **2** and its related MOs are provided in the Supporting Information.

tions of the frontier orbitals containing significant d-orbital character map well with those we have sketched qualitatively in Figure 2, although the SOMO is predicted by DFT to lie much closer in energy to the lower set of orbitals than to the LUMO. The SOMO and LUMO orbitals are nearly orthogonal to one another and align reasonably well along the plane containing the Co–O–Si vector. The lowest-lying three orbitals consist of one orbital of d_{z^2} -parentage (HOMO–2) and two

(48) Gütlich, P.; Garcia, Y.; Goodwin, H. A. *Chem. Soc. Rev.* **2000**, *29*, 419–427.

Table 4. Experimental and Calculated Bond Lengths and Angles for **2**, **6**, and **{16}**

2	exptl	calcd	6	exptl	calcd	{16}	exptl	calcd
Bond Lengths (Å)								
Co–O	1.799	1.849	Co–S	2.167	2.223	Co–O	1.766	1.776
Co–P1	2.156	2.429	Co–P1	2.251	2.418	Co–P1	2.187	2.236
Co–P2	2.284	2.224	Co–P2	2.199	2.271	Co–P2	2.182	2.241
Co–P3	2.169	2.251	Co–P3	2.208	2.286	Co–P3	2.184	2.234
Bond Angles (deg)								
Co–O–Si	172.5	162.8	Co–S–C46	114.6	119.1	Co–O–Si	178.6	178.7
P1–Co–P2	91.38	88.9	P1–Co–P2	89.44	89.4	P1–Co–P2	90.67	90.8
P1–Co–P3	85.88	94.8	P1–Co–P3	100.23	95.9	P1–Co–P3	90.18	90.8
P2–Co–P3	94.60	88.8	P2–Co–P3	86.73	89.5	P2–Co–P3	90.50	90.5
P1–Co–O	129.45	116.7	P1–Co–S	96.48	99.9	P1–Co–O	125.6	124.4
P2–Co–O	119.42	138.2	P2–Co–S	147.37	145.4	P2–Co–O	124.4	126.4
P3–Co–O	125.82	118.1	P3–Co–S	123.30	122.1	P3–Co–O	124.8	123.5

orbitals that are canted away from the Co–O–Si vector. While the low symmetry of the structure inevitably gives rise to d-orbital mixing, the lowest-lying pair of orbitals can be crudely described as d_{xy} and $d_{x^2-y^2}$ type orbitals, where the z -axis is assumed to be coincident with the Co–O–Si vector. Interestingly, there are two high-lying [BP₃]-centered orbitals (HOMO, HOMO–1) comprised within the frontier manifold that would have been difficult to anticipate in the absence of the calculation.

DFT-minimization of the geometry of **2** gives rise to a conformationally similar structure (**2**-DFT), with the noteworthy distinction that distortion of one of its Co–P bond distances is grossly exaggerated (2.22 Å, 2.25 Å, 2.43 Å). Despite this structural distinction, the calculation still points to a LUMO that is energetically well-separated from a lower-lying set of d-type orbitals that includes the SOMO. This conclusion is in accord with DFT studies for **6**. Table 4 compares the core bond lengths and angles of the calculated to the DFT determined structures.

Lobal representations of the frontier molecular orbitals of the off-axis thiolate complex **6** based upon a single-point electronic structure calculation are displayed in Figure 15. As can be gleaned, the LUMO is again energetically well-separated from a set of low-lying d-type orbitals. Certain comparative differences do arise with respect to the MO structure of **2**. The LUMO now appears to be coincident with the trigonal plane defined by two Co–P vectors and the Co–S vector, and the SOMO is directed with a lobe that is pointed toward the axial P donor ligand. The shape of the SOMO explains why the axial phosphine ligand is appreciably elongated in the crystal structure of **6**. The DFT-minimized structure, **6**-DFT, dramatically exaggerates this elongation, as was also observed for the case of **2**. The HOMO and HOMO–1 orbitals are no longer ligand centered but now comprise d-type orbitals with additional contributions from the equatorial thiolate ligand. The phasing suggests that the interaction is of Co–S π^* character in each case. The lowest-lying orbital is difficult to distinguish from the HOMO and HOMO–1 orbitals, and the high degree of mixing due to the low symmetry of the system is evident.

The transition state for dissociation of one phosphine ligand should look similar to the highly distorted structures we have calculated for **2** and **6**. In this context it is interesting to note that the d^7 low-spin half-sandwich complex TpCoCp* has been characterized and dissociation of one of its pyrazolyl donor arms is indeed observed in the solid state.^{9e,f} The authors have suggested that in solution an equilibrium between the κ^2 - and κ^3 -binding modes is present.^{9f} The crystal structure of **15** is

interesting for comparison in that it provides an experimentally determined ground-state structure featuring one Co–P bond that is strikingly elongated by comparison to the other two. In effect, the crystal structure of this complex is a better match for the theoretical structure obtained for **6**, and related d^7 [BP₃]Ni(NR) species,⁴¹ by virtue of the exaggerated distortion.⁴⁹ Because the solution magnetic (Evans) and EPR data for **15** are indicative of a high-spin component, it is reasonable to suggest that an equilibrium mixture between κ^2 - and κ^3 -binding modes might exist in solution. Nevertheless, it seems more likely to us that the equilibrium is between an umbrella distorted high-spin structure, similar to **8**, and an off-axis distorted low-spin structure in the solid state.

Our inability to faithfully reproduce the crystallographically determined structures of **2** and **6** detracts from our confidence to use DFT methods to theoretically predict the ground spin-state of these systems. To illustrate this point, when we calculate the total energy of the DFT-minimized structures of iodide **1** assuming a doublet and a quartet state, respectively, the quartet state is energetically favored by 8.8 kcal/mol. This result is in obvious contradiction to the experimentally observed low-spin state preference. A general problem associated with open-shell DFT calculations is that there is, as yet, no universally applicable method and basis-set that can be confidentially applied to a given system.³²

The geometries and electronic structures of closed-shell coordination complexes are more reliably predicted by current DFT methods, and we therefore examined diamagnetic **{16}**⁺. The nature of the SOMO orbital of **2** suggests that the removal of one unpaired electron should relieve its distorted structure. This is in fact observed, both crystallographically and theoretically. Recall that XRD analysis of **{16}**{BPh₄} revealed an extremely symmetric structure containing a P₃Co subunit defining one-half of an octahedron almost perfectly trisected by the Co–O–Si bond vector (Figure 5). **{16}**⁺ can be consequently classified by structure type **E** from Figure 2 and its molecular orbital diagram is therefore anticipated to reflect the two-over-three splitting diagram of an octahedral complex. The presence of degenerate π -bonding should give rise to a sizable separation between the upper two and lower three d-orbitals. This picture is evident from the single-point electronic

(49) We very recently obtained the solid-state crystal structure of the low-spin half-sandwich complex [PhBP₃]CoCp. While a thorough discussion of this and related [BP₃]-supported half-sandwich complexes is beyond the scope of this report, we note that in the crystalline state [PhBP₃]CoCp features a κ^3 -bonding mode of the [PhBP₃] ligand and features one Co–P bond distance that is extremely distorted (2.479 Å) by comparison to the other two Co–P bond distances (2.242 and 2.231 Å).

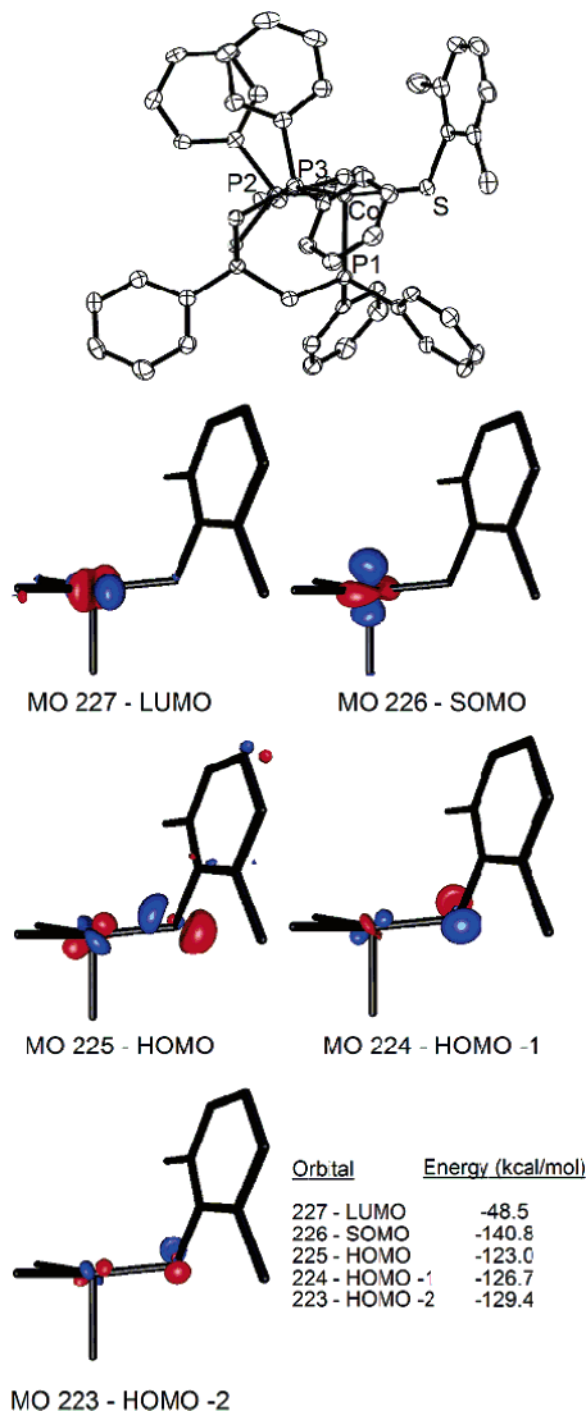


Figure 15. Molecular orbitals derived from a single-point energy DFT calculation of [PhBP₃]CoS(2,6-Me₂-Ph) (**6**) assuming a doublet ground state and the crystallographically determined atomic coordinates. The DFT minimized structure of **6** and its related MOs are provided in the Supporting Information.

structure calculation performed for {**16**}⁺. Lobar representations for the orbitals of dominant d-type contributions are shown in Figure 16. As for the MO structure of **2**, a number of filled ligand centered orbitals lie at relatively high energy, in this case falling between the lower-lying (a₁ + e) filled d-orbital set composed of d_{z²}, d_{xy}, and d_{x²-y²} and the upper-lying, empty d-orbital e set comprising d_{xz} and d_{yz}. These frontier d-orbitals reflect the unmistakable analogy between pseudotetrahedral {**16**}⁺ and the electronic structure of sandwich and half-

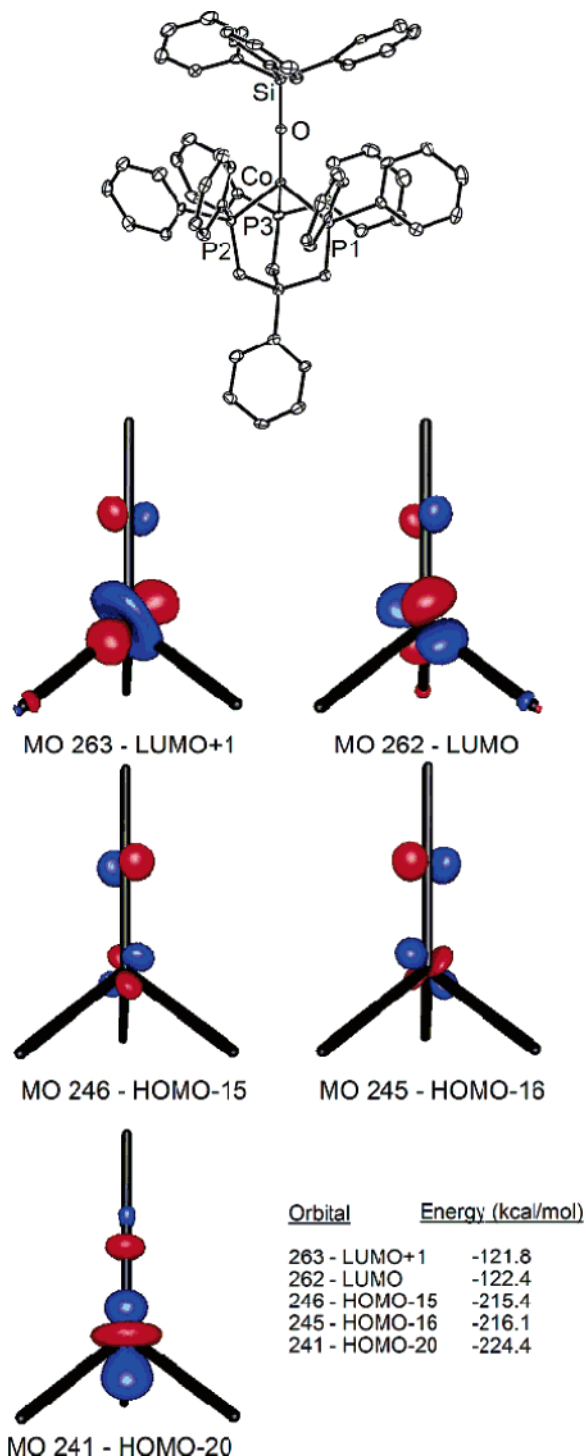


Figure 16. Molecular orbitals consisting of significant d-orbital contributions for the frontier region of {**16**}⁺. Orbitals were derived from a single-point electronic structure calculation assuming a singlet ground state and the crystallographically determined atomic coordinates.

sandwich complexes.^{9f,50} The DFT-optimized structure for {**16**}⁺ was found to be in good agreement with the crystal structure of {**16**}{BPh₄} (see Supporting Information and Table 4).

Concluding Remarks

It is evident from the present study that magnetic phenomena for distorted tetrahedral d⁷ ions can be much richer than had

(50) Sohn, Y. S.; Hendrickson, D. N.; Gray, H. B. *J. Am. Chem. Soc.* **1971**, *93*, 3603–3612.

been appreciated previously. For highly covalent [BP₃]Co(II) complexes, low-spin, high-spin, and spin-crossover complexes are readily accessible for a variety of related geometries best described as pseudotetrahedral with an umbrella or off-axis distortion. The observation of an $S = 1/2$ ground state for four-coordinate [BP₃]Co^{II}X complexes appears at this stage to be neither exceptional nor uncommon – a host of such complexes have now been thoroughly characterized. Given this situation, it is of obvious interest to re-examine other d⁷ L₃CoX scaffolds to determine whether access to the $S = 1/2$ ground state will prove more ubiquitous than was previously thought. Four-coordinate L₃Co^{II}–SR thiolate complexes should offer a good starting point in this regard, although for the single [Tp]Co(II) thiolate we have examined herein the more typical $S = 3/2$ ground state is preferred.

Our data establish that ground spin-state assignments for these types of d⁷ ions can be readily made by inspection of their low-temperature solid-state structural, SQUID, and EPR data. The halide structures [PhBP₃]CoI and [PhBPⁱPr₃]CoCl represent the simplest limiting cases.^{15,25} For example, the crystal structure of [PhBP₃]CoI reveals its $S = 1/2$ ground state by virtue of its three relatively short Co–P distances, with one bond longer than the other two. This contrasts with the structure of [PhBPⁱPr₃]CoCl, in which each Co–P distance is elongated but essentially equidistant and a three-fold axis is more readily discerned. The collection of low-temperature data collected for complexes **3** and **4** serve as a reminder that SQUID or EPR data need to be interpreted cautiously in the absence of structural data. In particular, slippage of a monodentate X-type ligand to a higher coordination mode (e.g., from η¹ to η³) can confer a spin-state change.

Curious and perhaps still counterintuitive is that the stronger-field donor ligand [PhBPⁱPr₃] tends to confer the high-spin configuration. Such is the case not only for [PhBPⁱPr₃]CoCl, but also for [PhBPⁱPr₃]CoI (**13**) and [PhBPⁱPr₃]CoOSiPh₃ (**14**). To account for this, we maintain that conformational constraints imposed by the [PhBPⁱPr₃] ligand will disfavor short Co–P contacts so as to minimize steric repulsion by the isopropyl groups of this bulky ligand. In the absence of overriding factors, such as strong π-bonding at the X-linkage, a high-spin population is energetically preferred. By choosing a more strongly π-donating X-type linkage, as is the case for the complex [PhBPⁱPr₃]CoSSiPh₃ (**15**), an $S = 1/2$ ground state can be realized (at least in the solid state), but now the requisite distortion that relieves the σ* (and appreciably π*) interaction of the SOMO is far more pronounced than for the case of low-spin [PhBP₃] systems, presumably alleviating repulsive steric interactions.

While these examples illustrate the effect that rather dramatic structural and electronic differences can have on the observed ground spin-states of these systems, more subtle differences can have equally striking consequences. For instance, the complex [PhBP₃]CoS(2,4,6-*i*-Pr₃-Ph) (**7**) is an off-axis low-spin species, whereas [PhBP₃]CoS(2,4,6-*i*-Bu₃-Ph) (**8**) adopts a distinctly different umbrella distortion and populates a high-spin ground state. Even more subtle changes can have profound electronic consequences. Replacement of the trityl C-atom in [PhBP₃]CoOCPH₃ (**12**) by the Si-atom in [PhBP₃]CoOSiPh₃ (**2**) alters the system's ground electronic state from $S = 3/2$ to $S = 1/2$, respectively. This secondary sphere effect is striking, and is immediately evident by comparison of the low-temperature

glassy toluene EPR spectra of the two species. We have also found that the spin population of a d⁷ L₃CoX system can be fine-tuned by adjusting the electron-donor character of the X-type linkage at a site even further removed from the cobalt center. This is evident from the SQUID magnetization and EPR data for [PhBP₃]CoOSi(4-NMe₂-Ph)₃ (**10**) and [PhBP₃]CoOSi(4-CF₃-Ph)₃ (**11**), and moreover suggests that truly cooperative spin-crossover d⁷ L₃CoX platforms might be realized if X-type linkages can be appropriately tailored. This possibility represents an exciting opportunity, as it would enable the reactivity patterns of structurally related $S = 1/2$ and $S = 3/2$, coordinatively unsaturated d⁷ ions to be probed as a function of their spin populations.^{32c,51}

Experimental Section

All manipulations were carried out using standard Schlenk or glovebox techniques under a dinitrogen atmosphere. Unless otherwise noted, solvents were deoxygenated and dried by thorough sparging with N₂ gas, followed by passage through an activated alumina column. Diethyl ether, tetrahydrofuran, petroleum ether, benzene, and toluene were periodically tested with a standard purple solution of sodium benzophenone ketyl in tetrahydrofuran to confirm that oxygen and moisture had been effectively removed. The preparation of [PhBP₃]CoI (**1**),^{14,15} {[PhBP₃]CoCl},¹⁵ [PhBP₃]CoOSiPh₃ (**2**),¹⁶ and [PhBPⁱPr₃]CoI (**13**)²⁵ has been previously reported. The reagents TiOSiPh₃,⁵² TiO-*p*-*t*-Bu-Ph,³⁹ TISPh,⁵³ HS(2,4,6-*i*-Pr₃-Ph),⁵⁴ HS(2,4,6-*i*-Bu₃-Ph),⁵⁵ HOSi(*p*-NMe₂-Ph)₃,⁵⁶ HOSi(*p*-CF₃-Ph)₃,⁵⁷ [Cp₂Fe][BPh₄],⁵⁸ and [Cp₂Fe][B(3,5-(CF₃)₂-Ph)₄]⁵⁹ were prepared according to literature procedures. TiO(C₆F₅), TIS(2,6-Me₂-Ph), TIS(2,4,6-*i*-Pr₃-Ph), TIS(2,4,6-*i*-Bu₃-Ph), TISSiPh₃, TiOCPH₃, TiOSi(*p*-NMe₂-Ph)₃, and TiOSi(*p*-CF₃-Ph)₃ were prepared via a modification of a general synthetic method reported by Tolman (see below).³⁹ The reagents HO(*p*-*t*-Bu-Ph), HO(C₆F₅), HSPH, HS(2,6-Me₂-Ph), HOCPh₃, HOSiPh₃, HSSiPh₃, CoBr₂, and [K][Tp^{3,5-Me2}] were purchased from commercial vendors and used without further purification. Thallium ethoxide was purchased from Aldrich, filtered through a pad of Celite to remove insoluble black material, and then stored at –35 °C. Elemental analyses were performed by Desert Analytics, Tucson, AZ. A Varian Mercury-300 NMR spectrometer or a Varian Inova-500 NMR spectrometer was used to record ¹H, ³¹P, and ¹⁹F NMR spectra at ambient temperature. ¹H chemical shifts were referenced to residual solvent. ³¹P NMR chemical shifts are referenced to an external standard of H₃PO₄ with the ³¹P signal being set at 0 ppm. ¹⁹F NMR chemical shifts are referenced to an external standard of neat hexafluorobenzene with the ¹⁹F signal being set at –163 ppm. Deuterated toluene, benzene, and tetrahydrofuran were purchased from Cambridge Isotope Laboratories, Inc. and were degassed and dried over activated 3 Å molecular sieves prior to use. UV–vis measurements were obtained using a Varian Cary 50 Bio using a quartz crystal cell equipped with a Teflon cap. UV–vis–NIR measurements were taken in C₆D₆ on a Cary 500 spectrophotometer using a 1 mm path length quartz crystal

- (51) Poli, R. *Chem. Rev.* **1996**, *96*, 2135–2204.
- (52) Harvey, S.; Lappert, M. F.; Raston, C. L.; Skelton, B. W.; Srivastava, G.; White, A. H. *J. Chem. Soc., Chem. Commun.* **1988**, *17*, 1216–1217.
- (53) Dettly, M. R.; Wood, G. P. *J. Org. Chem.* **1980**, *45*, 80–89.
- (54) (a) Oae, S.; Togo, H. *Bull. Chem. Soc. Jpn.* **1983**, *56*, 3802–3812. (b) Blower, P. J.; Dilworth, J. R.; Hutchinson, J. P.; Zubieta, J. A. *J. Chem. Soc., Dalton Trans.* **1975**, 1533–1541.
- (55) Bochmann, M.; Webb, K. J. *Inorg. Synth.* **1997**, *31*, 158–162.
- (56) Gilman, H.; Plunkett, M. A.; Dunn, G. E. *J. Am. Chem. Soc.* **1951**, *73*, 1686–1688. Trichlorosilane was substituted for tetrachlorosilane.
- (57) HOSi(*p*-CF₃-Ph) was prepared by the method of: Pauling, H.; Andrews, D. A.; Hindley, N. C. *Helv. Chim. Acta* **1976**, *59*, 1233–1243.
- (58) (a) Connelly, N. G.; Geiger, W. E. *Chem. Rev.* **1996**, *96*, 877–910. (b) Jordan, R. F.; LaPointe, R. E.; Bajgur, C. S.; Echols, S. F.; Willett, R. J. *Am. Chem. Soc.* **1987**, *109*, 4111–4113. (c) Aggarwal, R. P.; Connelly, N. G.; Crespo, M. C.; Dunne, B. J.; Hopkins, P. M.; Orpen, A. G. *J. Chem. Soc., Dalton Trans.* **1992**, 655–662.
- (59) Le Bras, J.; Jiao, H.; Meyer, W. E.; Hampel, F.; Gladysz, J. A. *J. Organomet. Chem.* **2000**, *616*, 54–66.

cell equipped with a Teflon cap. X-ray diffraction experiments were carried out by the Beckman Institute Crystallographic Facility on a Bruker Smart 1000 CCD diffractometer. Cyclic voltammetry measurements were made inside a dry glovebox using a BAS 100 electrochemical analyzer with a glassy carbon working electrode, platinum wire counter electrode, and Ag/AgNO₃ reference electrode. All potentials were measured versus an external standard of ferrocene.

Magnetic Measurements. Measurements were recorded using a Quantum Designs SQUID magnetometer running MPMSR2 software (Magnetic Property Measurement System revision 2). Data were recorded at 5000 G. Samples were suspended in the magnetometer in plastic straws sealed under nitrogen with Lilly no. 4 gel caps. Loaded samples were centered within the magnetometer using the DC centering scan at 35 K and 5000 gauss. Data were acquired at 4–30 K (one data point every 2 K), 30–300 K (one data point every 5 K).

$$\chi_m = \frac{\chi M}{mG} \quad (3)$$

$$\mu_{\text{eff}} = \sqrt{7.997\chi_m T} \quad (4)$$

The magnetic susceptibility was adjusted for diamagnetic contributions using the constitutive corrections of Pascal's constants.⁶⁰ The molar magnetic susceptibility (χ_m) was calculated by converting the calculated magnetization (χ) obtained from the magnetometer to a molar susceptibility (using the multiplication factor {(molecular weight)/[(sample weight)(field strength)]}). Data were analyzed using eqs 3 and 4. Solution magnetic moments were measured by the method of Evans⁶¹ and were adjusted for diamagnetic contributions using the constitutive corrections of Pascal's constants.

EPR Measurements. X-band EPR spectra were obtained on a Bruker EMX spectrometer equipped with a rectangular cavity working in the TE₁₀₂ mode. Variable-temperature measurements were conducted with an Oxford continuous-flow helium cryostat (temperature range 3.6–300 K). Accurate frequency values were provided by a frequency counter built in the microwave bridge. Solution spectra were acquired in toluene. Sample preparation was performed under a nitrogen atmosphere. Specific experimental parameters for each spectra presented can be found in the Supporting Information.

Computational Methods. All calculations were performed using the hybrid DFT functional B3LYP as implemented in the Jaguar 5.0 program package.⁶² This DFT functional utilizes the Becke three-parameter functional⁶³ (B3) combined with the correlation functional of Lee, Yang, and Parr⁶⁴ (LYP). LACVP** was used as the basis set. Input coordinates were derived as described in the text from crystallographically determined structures. Spin-states and molecular charges were explicitly stated, and no molecular symmetry was imposed. Default values for geometry and SCF iteration cutoffs were used. All structures converged under these criteria except for the geometry minimization of **2**. In this case, multiple additional cycles showed no more than 1 kcal/mol difference in energy.

The continuous symmetry measurements were determined with the program SHAPE developed at the Universitat de Barcelona, Spain.⁶⁵

General Method for the Preparation of Thallium Reagents (modified from Tolman et al.).³⁹ The appropriate phenol, thiol, silanol, or silylthiol (about 200 mg) was dissolved in petroleum ether (10 mL) and a minimal amount of THF (if necessary). One equivalent of thallium ethoxide was added as a petroleum ether solution (4 mL), and the reaction mixture was stirred for 30 min. The reaction was performed

in the dark to minimize thallium ethoxide degradation. The precipitates were collected on a medium frit and washed with petroleum ether (2 × 10 mL) and then dried. The thallium reagents were used without further purification.

Additional ¹H NMR data for [PhBP₃]CoI, **1:** ¹H NMR (C₆D₆, 300 MHz): δ 22.3 (6 H, $T_1 = 2.4$ ms, PhB(CH₂PPh₂)₃), 10.8 (12 H, $T_1 = 23.6$ ms, *m*-P(C₆H₅)₂), 7.7 (2 H, $T_1 = 40.5$ ms, *o*-B(C₆H₅)), 7.5 (3 H, $T_1 = 205$ ms, *m*- and *p*-B(C₆H₅)), 4.3 (12 H, $T_1 = 1.2$ ms, *o*-P(C₆H₅)₂), 2.2 (6 H, $T_1 = 46.7$ ms, *p*-P(C₆H₅)₂).

Synthesis of [PhBP₃]CoOSiPh₃, **2.** A THF (4 mL) solution of TIOSiPh₃ (0.173 g, 0.361 mmol) was added dropwise to a stirring solution of [PhBP₃]CoI (**1**) (0.315 g, 0.361 mmol) in THF (8 mL). The resulting solution was allowed to stir for 10 h. An orange precipitate formed (TII) which was filtered away over diatomaceous earth. The THF was then removed in vacuo, and the resulting solid was dissolved in benzene (4 mL). Crystals were grown from vapor diffusion of petroleum ether into a benzene solution. The purple crystals were dried and weighed (0.300 g, 81% yield). The crystals were recrystallized two additional times (from benzene/petroleum ether) before measurements were taken on the samples (95% yield for each recrystallization). ¹H NMR (C₆D₆, 300 MHz): δ 15.6, 10.0, 9.8, 8.6, 8.3, 7.4, 1.1 (br), -2.2. ¹H NMR (*d*₈-toluene, 300 MHz): δ 15.4, 9.9, 9.7, 8.6, 8.1, 7.4 (m), 7.1 (m), 1.1 (br), -2.0. UV-vis (C₆D₆) λ_{max} , nm (ϵ): 557 (700), 763 (310). UV-vis (C₆D₆) λ_{max} , nm (ϵ): 557 (670), 757 (280), 1136 (320). UV-vis (toluene) λ_{max} , nm (ϵ): 557 (650), 763 (290). UV-vis (THF) λ_{max} , nm (ϵ): 557 (670), 761 (300). Evans' Method (C₆D₆, 295 K): 3.4 μ_B ; (*d*₈-toluene, 295 K): 3.5 μ_B ; (*d*₈-THF, 295 K): 3.5 μ_B . EPR (toluene, 20 K): $g_x = 2.03$, $a_{x(\text{Co})} = 65$ G, $a_{x(\text{P})} = 34$ G; $g_y = 2.05$, $a_{y(\text{Co})} = 12$ G, $a_{y(\text{P})} = 27$ G; $g_z = 2.21$, $a_{z(\text{Co})} = 105$ G, $a_{z(\text{P})} = 28$ G. Electrochemistry (vs ferrocene in THF with [TBA][ClO₄] as supporting electrolyte): Co^{III}/Co^{II}, -360 mV; Co^{II}/Co^I, -1290 mV. Anal. Calcd for C₆₃H₅₆BCoOP₃Si: C, 74.19; H, 5.53. Found: C, 74.27; H, 5.42.

Synthesis of [PhBP₃]CoO(4-Bu-Ph), **3.** Followed protocol for **2**. Used TIO-*p*-Bu-Ph (85.8 mg, 0.243 mmol) and **1** (212 mg, 0.243 mmol). Red-brown crystals of **3** were isolated (115 mg, 53% yield). ¹H NMR (C₆D₆, 300 MHz): δ 12.3 (br), 9.2, 7.7, 2.1, 1.2, 0.9, 0.5 (br). UV-vis (C₆H₆) λ_{max} , nm (ϵ): 428 (2300), 567 (1600), 715 (700). Evans' Method (C₆D₆): 3.4 μ_B . Electrochemistry (vs ferrocene in THF with [TBA][PF₆] as supporting electrolyte): Co^{III}/Co^{II}, -390 mV; Co^{II}/Co^I, -1330 mV. Anal. Calcd for C₅₅H₅₄BCoOP₃: C, 73.92; H, 6.09. Found: C, 73.58; H, 6.01.

Synthesis of [PhBP₃]CoO(C₆F₅), **4.** Followed protocol for **2**. Used TIO(C₆F₅) (109 mg, 0.281 mmol) and **1** (245 mg, 0.281 mmol). Olive green crystals of **4** were isolated (159 mg, 59% yield). ¹H NMR (C₆D₆, 300 MHz): δ 16.9, 10.9, 8.5, 7.5, -1.0, -3.4, -61.8. ¹⁹F NMR (C₆D₆, 282 MHz): δ -73.1, -181.0. UV-vis (C₆H₆) λ_{max} , nm (ϵ): 582 (740), 712 (560). Evans' Method (C₆D₆): 3.8 μ_B . Anal. Calcd for C₅₁H₄₁BCoF₅OP₃: C, 66.04; H, 4.46. Found: C, 65.19; H, 4.39.

Synthesis of [PhBP₃]CoSPh, **5.** Followed protocol for **2**. Used TISPh (94.0 mg, 0.300 mmol) and **1** (261 mg, 0.300 mmol). Red crystals of **5** were isolated (193 mg, 75% yield). ¹H NMR (C₆D₆, 300 MHz): δ 24.7 (br), 16.7, 10.7, 8.3, 7.7, 7.6, 2.2 (br), 1.4, -3.1 (br), -6.0. UV-vis (C₆D₆) λ_{max} , nm (ϵ): 460 (3500), 597 (1800), 1204 (270). Evans' Method (C₆D₆): 2.4 μ_B . Electrochemistry (vs ferrocene in THF with [TBA][PF₆] as supporting electrolyte): Co^{III}/Co^{II}, -160 mV; Co^{II}/Co^I, -1120 mV. Anal. Calcd for C₅₁H₄₆BCoP₃S: C, 71.76; H, 5.43. Found: C, 71.94; H, 5.42.

Synthesis of [PhBP₃]CoS(2,6-Me₂-Ph), **6.** Followed protocol for **2**. Used TIS(2,6-Me₂-Ph) (102 mg, 0.297 mmol) and **1** (259 mg, 0.297 mmol). Red crystals of **6** were isolated (172 mg, 66% yield). ¹H NMR (C₆D₆, 300 MHz): δ 79.8, 26.7, 19.6, 13.1, 9.9, 8.2, 8.0, 0.5 (br), -1.1, -21.1. UV-vis (C₆H₆) λ_{max} , nm (ϵ): 396 (4600), 486 (3200), 599 (2300), 741 (900). Evans' Method (C₆D₆): 2.3 μ_B . Electrochemistry (vs ferrocene in THF with [TBA][ClO₄] as supporting electrolyte):

(60) Kahn, O. *Molecular Magnetism*; VCH Publishers: New York, 1993; pp 1–86.

(61) (a) Sur, S. K. *J. Magn. Reson.* **1989**, *82*, 169–173. (b) Evans, D. F. *J. Chem. Soc.* **1959**, 2003–2005.

(62) *Jaguar 5.0*, Schrodinger, LLC, Portland, Oregon, 2002.

(63) Becke, A. D. *J. Chem. Phys.* **1993**, *98*, 5648–5652.

(64) Lee, C.; Yang, W.; Parr, R. G. *Phys. Rev. B* **1988**, *37*, 785–789.

(65) Llunell, M.; Casanova, D.; Cirera, J.; Bofill, J. M.; Alemany, P.; Alvarez, S.; Pinsky, M.; Avnir, D. *SHAPE*, version 1.1; Barcelona, 2003.

$\text{Co}^{\text{III}}/\text{Co}^{\text{II}}$, -170 mV; $\text{Co}^{\text{II}}/\text{Co}^{\text{I}}$, -1100 mV. Anal. Calcd for $\text{C}_{53}\text{H}_{50}\text{BCoP}_3\text{S}$: C, 72.20; H, 5.72. Found: C, 72.42; H, 5.69.

Synthesis of [PhBP₃]CoS(2,4,6-*i*-Pr₃-Ph), 7. Followed protocol for 2. Used TIS(2,4,6-*i*-Pr₃-Ph) (117 mg, 0.265 mmol) and {[PhBP₃]CoCl} (207 mg, 0.265 mmol). Red-brown crystals of 7 were isolated (178 mg, 68% yield). ¹H NMR (C_6D_6 , 300 MHz): δ 46.4 (br), 21.7, 11.6, 9.1, 8.9, 7.8, 7.7, 4.8, 1.3, 0.9. UV-vis (C_6H_6) λ_{max} , nm (ϵ): 384 (6600), 471 (4200), 609 (3000), 743 (900). Evans' Method (C_6D_6): 2.8 μB . Electrochemistry (vs ferrocene in THF with [TBA][PF₆] as supporting electrolyte): $\text{Co}^{\text{III}}/\text{Co}^{\text{II}}$, -80 mV; $\text{Co}^{\text{II}}/\text{Co}^{\text{I}}$, -1190 mV. Anal. Calcd for $\text{C}_{60}\text{H}_{64}\text{BCoP}_3\text{S}$: C, 73.54; H, 6.58. Found: C, 73.18; H, 6.57.

Synthesis of [PhBP₃]CoS(2,4,6-*t*-Bu₃-Ph), 8. Followed protocol for 2. Used TIS(2,4,6-*t*-Bu₃-Ph) (145 mg, 0.302 mmol) and 1 (263 mg, 0.302 mmol). Red crystals of 8 were isolated (113 mg, 36% yield). ¹H NMR (C_6D_6 , 300 MHz): δ 50.8, 16.7, 12.8, 10.6 (br), 9.2, 8.1, 2.3, -3.2 (br), -5.4 , -27.0 . UV-vis (C_6D_6) λ_{max} , nm (ϵ): 479 (3600), 640 (1900), 754 (1800), 1190 (430). Evans' Method (C_6D_6): 3.9 μB . Electrochemistry (vs ferrocene in THF with [TBA][PF₆] as supporting electrolyte): $\text{Co}^{\text{III}}/\text{Co}^{\text{II}}$, -60 mV; $\text{Co}^{\text{II}}/\text{Co}^{\text{I}}$, -1080 mV. Anal. Calcd for $\text{C}_{63}\text{H}_{70}\text{BCoP}_3\text{S}$: C, 74.04; H, 6.90. Found: C, 73.95; H, 6.98.

Synthesis of [PhBP₃]CoSSiPh₃, 9. Followed protocol for 2. Used TISSiPh₃ (187 mg, 0.376 mmol) and 1 (328 mg, 0.376 mmol). Green crystals of 9 were isolated (321 mg, 83% yield). ¹H NMR (C_6D_6 , 300 MHz): δ 46.4, 11.9, 8.7–6.6, 1.3. UV-vis (C_6H_6) λ_{max} , nm (ϵ): 622 (1300), 747 (670). Evans' Method (C_6D_6): 2.5 μB . Electrochemistry (vs ferrocene in THF with [TBA][PF₆] as supporting electrolyte): $\text{Co}^{\text{III}}/\text{Co}^{\text{II}}$, -210 mV (irreversible), $\text{Co}^{\text{II}}/\text{Co}^{\text{I}}$, -1010 mV. Anal. Calcd for $\text{C}_{63}\text{H}_{56}\text{BCoP}_3\text{SSi}$: C, 73.04; H, 5.45. Found: C, 73.06; H, 5.49.

Synthesis of [PhBP₃]CoOSi(4-NMe₂-Ph)₃, 10. Followed protocol for 2. Used TIOSi(*p*-NMe₂-Ph)₃ (228 mg, 0.374 mmol) and {[PhBP₃]CoCl} (292 mg, 0.374 mmol). Layering of petroleum ether (14 mL) onto a toluene solution (4 mL) afforded red crystalline product (173 mg). The recrystallization of the supernatant leads to additional product (115 mg) to give a total yield of 67%. ¹H NMR (C_6D_6 , 300 MHz): δ 103.7, 14.6, 10.1 (br), 9.5, 8.1, 7.8, 7.4, 2.7, 2.1, -1.0 . UV-vis (C_6H_6) λ_{max} , nm (ϵ): 555 (940), 699 (440), 772 (420). Evans' Method (C_6D_6): 3.5 μB . Electrochemistry (vs ferrocene in THF with [TBA][ClO₄] as supporting electrolyte): $\text{Co}^{\text{III}}/\text{Co}^{\text{II}}$, -360 mV; $\text{Co}^{\text{II}}/\text{Co}^{\text{I}}$, -1300 mV. Anal. Calcd for $\text{C}_{69}\text{H}_{71}\text{BCoN}_3\text{OP}_3\text{Si}$: C, 72.12; H, 6.23; N, 3.66. Found: C, 71.77; H, 6.40; N, 3.52.

Synthesis of [PhBP₃]CoOSi(4-CF₃-Ph)₃, 11. Followed protocol for 2. Used TIOSi(*p*-CF₃-Ph)₃ (99 mg, 0.145 mmol) and {[PhBP₃]CoCl}, (113 mg, 0.145 mmol). The toluene solution (2 mL) was layered with 15 mL of petroleum ether and cooled to -35 °C until crystals formed. The crystals were then dried in vacuo yielding the pure compound (117 mg, 66% yield). ¹H NMR (C_6D_6 , 300 MHz): δ 17.4, 10.7, 9.8 (br), 8.8, 8.5, 7.3, -0.9 , -4.2 , -81.6 (br). ¹⁹F NMR (C_6D_6 , 282 MHz): δ -58.1 . UV-vis (C_6H_6) λ_{max} , nm (ϵ): 560 (740), 757 (320). Evans' Method (C_6D_6 , 298 K): 3.9 μB . Electrochemistry (vs ferrocene in THF with [TBA][ClO₄] as supporting electrolyte): $\text{Co}^{\text{III}}/\text{Co}^{\text{II}}$, -60 mV (irreversible), $\text{Co}^{\text{II}}/\text{Co}^{\text{I}}$, -1080 mV. Anal. Calcd for $\text{C}_{66}\text{H}_{53}\text{BCoF}_9\text{OP}_3\text{Si}$: C, 64.77; H, 4.36. Found: C, 64.70; H, 4.55.

Synthesis of [PhBP₃]CoOCPh₃, 12. A THF solution (3 mL) of the thallium reagent TIOCPPh₃ (124 mg, 0.267 mmol) was added to a stirring THF solution (10 mL) of [PhBP₃]CoI, 1, (233 mg, 0.267 mmol). The solution was stirred for 4 h, and a yellow precipitate formed (TII). The precipitate was removed by filtration over diatomaceous earth. The remaining reaction volatiles were removed in vacuo, and the blue/green powder was then washed with petroleum ether (2 \times 10 mL) and dried. The solid was then reconstituted in benzene (4 mL) and then triturated with petroleum ether (15 mL). The supernatant was separated from the brown solid via filtration. The blue/green solution was dried in vacuo and then crystallized by vapor diffusion of petroleum ether into a benzene solution (47 mg, 18% yield). ¹H NMR (C_6D_6 , 300 MHz): δ 20.1, 16.7, 11.3, 9.5, 8.7, 7.9, 7.7, -1.4 , -5.0 , -83.7 . UV-vis (C_6H_6) λ_{max} , nm (ϵ): 578 (550), 778 (270). Evans' Method (C_6D_6 , 298 K):

3.8 μB . Electrochemistry (vs ferrocene in THF with [TBA][PF₆] as supporting electrolyte): $\text{Co}^{\text{III}}/\text{Co}^{\text{II}}$, -300 mV; $\text{Co}^{\text{II}}/\text{Co}^{\text{I}}$, -1310 mV. Anal. Calcd for $\text{C}_{64}\text{H}_{56}\text{BCoOP}_3$: C, 76.58; H, 5.62. Found: C, 76.23; H, 5.88.

Additional ¹H NMR data for [PhBP^{*i*}Pr₃]CoI, 13: ¹H NMR (C_6D_6 , 300 MHz): δ 115.6 (6 H, $T_1 = 2.6$ ms, PhB(CH₂P^{*i*}Pr₂)₃ or P(CH(CH₃)₂)₂), 41.6 (6 H, $T_1 = 0.9$ ms, PhB(CH₂P^{*i*}Pr₂)₃ or P(CH(CH₃)₂)₂), 24.1 (18 H, $T_1 = 5.6$ ms, P(CH(CH₃)₂)₂), 12.8 (2 H, $T_1 = 17.5$ ms, *o*-B(C₆H₅)), 9.0 (1 H, $T_1 = 204$ ms, *p*-B(C₆H₅)), 7.3 (2 H, $T_1 = 244$ ms, *m*-B(C₆H₅)), 3.3 (18 H, $T_1 = 1.9$ ms, P(CH(CH₃)₂)₂).

Synthesis of [PhBP^{*i*}Pr₃]CoOSiPh₃, 14. A THF solution (2 mL) of the thallium reagent TIOSiPh₃ (58 mg, 0.12 mmol) was added to a stirring THF solution (5 mL) of [PhBP^{*i*}Pr₃]CoI, 13, (81 mg, 0.12 mmol). The solution was stirred for 1 h, and a yellow precipitate formed (TII). The precipitate was removed by filtration over diatomaceous earth. The remaining reaction volatiles were removed in vacuo, and the purple powder was redissolved in benzene (5 mL). The benzene solution was filtered over diatomaceous earth to remove any residual TII and then frozen and lyophilized to remove any trace of THF. Vapor diffusion of petroleum ether into a benzene solution (1 mL) afforded purple crystalline product (39 mg, 41% yield). ¹H NMR (C_6D_6 , 300 MHz): δ 32.8, 21.6, 12.1, 11.0, 9.2, 8.9, 7.5, 7.4, 1.7, -60.3 . UV-vis (C_6H_6) λ_{max} , nm (ϵ): 553 (600), 657 (380), 788 (320). Evans' Method (C_6D_6): 4.3 μB . Electrochemistry (vs ferrocene in THF with [TBA][PF₆] as supporting electrolyte): $\text{Co}^{\text{III}}/\text{Co}^{\text{II}}$, 100 mV (irreversible); $\text{Co}^{\text{II}}/\text{Co}^{\text{I}}$, -1690 mV. Anal. Calcd for $\text{C}_{45}\text{H}_{68}\text{BCoOP}_3\text{Si}$: C, 66.25; H, 8.40. Found: C, 66.20; H, 8.14.

Synthesis of [PhBP^{*i*}Pr₃]CoSSiPh₃, 15. Followed protocol for 14. Used TISSiPh₃ (161 mg, 0.325 mmol) and 13 (216 mg, 0.325 mmol). Green crystals of 15 were isolated (167 mg, 62% yield). ¹H NMR (C_6D_6 , 300 MHz): δ 35.7, 20.7, 11.4, 9.3, 8.7, 7.8, 7.1, 6.2, 5.0, -52.6 . UV-vis (C_6H_6) λ_{max} , nm (ϵ): 604 (420), 664 (520), 747 (1300). Evans' Method (C_6D_6): 4.0 μB . Electrochemistry (vs ferrocene in THF with [TBA][PF₆] as supporting electrolyte): $\text{Co}^{\text{III}}/\text{Co}^{\text{II}}$, -140 mV (irreversible), $\text{Co}^{\text{II}}/\text{Co}^{\text{I}}$, -1330 mV. Anal. Calcd for $\text{C}_{45}\text{H}_{68}\text{BCoP}_3\text{SSi}$: C, 64.97; H, 8.24. Found: C, 64.77; H, 8.28.

Synthesis of {[PhBP₃]CoOSiPh₃}{BAR₄}, {16}{BAR₄}. Solid [PhBP₃]CoOSiPh₃, 2, (98 mg, 0.096 mmol) and [Cp₂Fe][B(3,5-(CF₃)₂-Ph)₄] (101 mg, 0.096 mmol) were added to a 20-mL vial, and then THF (8 mL) was added. The solution immediately went from purple to green and was stirred for 10 min. The reaction mixture was then dried in vacuo to leave a green powder which was washed with petroleum ether (3 \times 10 mL). The green powder was dried to leave the pure product (140 mg, 77% yield) which was stored at -35 °C. A similar procedure was used with [Cp₂Fe][BPh₄] as the oxidant giving the less soluble counteranion (for X-ray crystallography). In this case the dried product was washed with a petroleum ether/benzene mixture (7:3) (3 \times 10 mL) to give the final product (51% yield). A single crystal was grown at -35 °C in CH₂Cl₂ using the {BPh₄} counteranion. For {16}{B(3,5-(CF₃)₂-Ph)₄}: ¹H NMR (C_6D_6 , 300 MHz): δ 8.43 (s, 8 H, *o*-B(3,5-(CF₃)₂-C₆H₃)₄), 7.81 (d, $J = 6.0$ Hz, 8 H, *o*-Si(C₆H₅)₃ and *o*-B(C₆H₅)), 7.67 (t, $J = 7.5$ Hz, 2 H, *m*-B(C₆H₅)), 7.60 (s, 4 H, *p*-B(3,5-(CF₃)₂-C₆H₃)₄), 7.47 (t, $J = 7.5$ Hz, 1 H, *p*-B(C₆H₅)), 7.28 (m, 9 H, *m*- and *p*-Si(C₆H₅)₃), 7.10 (m, 12 H, *o*-P(C₆H₅)₂), 6.67 (t, $J = 7.2$ Hz, 6 H, *p*-P(C₆H₅)₂), 6.40 (t, $J = 7.5$ Hz, 12 H, *m*-P(C₆H₅)₂), 0.98 (br s, 6 H, PhB(CH₂PPh₂)₃). ³¹P{¹H} NMR (C_6D_6 , 121.4 MHz): δ 64.6. ¹⁹F{¹H} NMR (C_6D_6 , 282 MHz): δ -58.5 . UV-vis (C_6D_6) λ_{max} , nm (ϵ): 624 (830). Anal. Calcd for $\text{C}_{95}\text{H}_{68}\text{B}_2\text{CoF}_{24}\text{OP}_3\text{Si}$: C, 60.59; H, 3.64. Found: C, 60.59; H, 4.00. For {16}{BPh₄}: Identical UV-vis and ³¹P NMR spectra were found for the substituted anion.

Synthesis of [Tp^{3,5-Me₂}]CoS(2,6-Me₂-Ph), 17. Following a related procedure,^{33a} anhydrous CoBr₂ (61.8 mg, 0.285 mmol) was suspended in THF (13 mL) for 10 min. Solid [K][Tp^{3,5-Me₂}] (0.113 g, 0.335 mmol) was added over 30 min. To this solution, TIS(2,6-Me₂-Ph) (0.114 g, 0.335 mmol) was added as a THF (3 mL) slurry and stirred for 30 min. After the addition of the thallium reagent, the solution turned green,

and white precipitate appeared (TlBr). The solution was filtered over Celite and then dried in vacuo to leave a green powder. The green powder was taken up in toluene (3 mL) and then crystallized by vapor diffusion of petroleum ether, giving green crystals (0.043 g, 31% yield). Additional crystallizations can be used to collect more product, giving 69% total yield. 1H NMR (C_6D_6 , 300 MHz): δ 68.1, 38.5, 29.4, 16.2, -0.8, -11.4, -38.8. UV-vis (C_6H_6) λ_{max} , nm (ϵ): 647 (1300). SQUID (10–300 K): $\chi T_{av} = 2.41$ cm³ K mol⁻¹. Anal. Calcd for $C_{23}H_{31}BCoN_6S$: C, 55.99; H, 6.33; N, 17.03. Found: C, 55.72; H, 6.23; N, 17.12.

Acknowledgment. Financial support from the NSF (CHE-0132216), the DOE (PECASE), and the Alfred P. Sloan Foundation is gratefully acknowledged. D.M.J. was supported by an NSF predoctoral fellowship. The Beckman Institute (Caltech) provided access to a SQUID magnetometer, and the

Zewail lab provided access to a NIR spectrophotometer. Dr. Michael Day and Larry Henling provided crystallographic assistance, and Dr. Angel Di Bilio provided EPR assistance. Finally, we are very grateful to Dr. Santiago Alvarez and Jordi Cirera (Universitat de Barcelona, Spain) for help with the continuous symmetry measurement analysis and a stimulating scientific exchange.

Supporting Information Available: Additional SQUID magnetization data and EPR spectra, experimental parameters for EPR spectra, theoretical details for **2**, **6**, and **{16}**⁺; detailed crystallographic data in CIF format. This material is free of charge via the Internet at <http://pubs.acs.org>.

JA045310M